WATER RESOURCES RESEARCH, VOL. 37, NO. 7, PAGES 1893–1912, JULY 2001

Concentration variance and spatial covariance in second-order stationary heterogeneous conductivity fields

Jan Vanderborght[1]

Laboratory for Soil and Water, Department of Land Management, Faculty of Applied Biological and Agricultural Science, Catholic University Leuven, Belgium

Abstract. The concentration variance and spatial covariance resulting from convective-dispersive transport driven by a uniform mean flow in second-order stationary conductivity fields was derived in a Lagrangian framework based on a first-order approximation of solute particle trajectories. The approximation of the concentration (co)variances for large injection volumes is considerably simplified by defining the concentration at a certain location $\mathbf{x}$ and time t in terms of the "backward" solute trajectory probability distribution. This is the probability that the trajectory of a fictitious microscopic and indivisible solute particle, which is in a volume $\Delta\mathbf{x}$ centered around $\mathbf{x}$ at time t, was at the time of solute injection, t_0, in the injection volume, $\mathbf{V_0}$. The approximated concentration (co)variances were validated against concentration covariances derived from transport simulations in generated second-order stationary conductivity fields. The approximate solutions reproduced fairly well the effects of local scale dispersion and of the spatial variability of the hydraulic conductivity on the concentration (co)variance. The effect of the spatial structure of the hydraulic conductivity field on the spatial covariance of the concentrations was investigated in order to identify parameters that can be unequivocally determined from the structure of the concentration field. For a given spreading of the solute plume in the mean flow direction, $X_{11}(t)$, a given spatial correlation length of the $\log_e$ transformed hydraulic conductivity in the transverse to flow direction, I_{f2}, and a given local scale dispersion $\mathbf{D_d}$ the concentration covariance was nearly invariant and hardly influenced by the anisotropy of the covariance function, e, and the variance, σ_f^2, of the $\log_e$ transformed conductivity. As a result, e and σ_f^2 cannot be unequivocally determined from the spatial structure of the concentration field. The concentration variance and spatial covariance in the transverse to mean flow direction are predominantly determined by the lateral component of the local scale dispersion, D_{d22}, and by the spatial correlation length of the $\log_e$ transformed conductivity in the transverse to flow direction, I_{f2}. These two parameters might be unequivocally derived from the concentration (co)variance.

1. Introduction

Solute transport in porous formations is largely influenced by the heterogeneous nature of the flow, which results from the spatial variability of the hydraulic conductivity. Relations between the spreading of a solute plume and the spatial variability of the hydraulic conductivity have been investigated quite intensively. First-order approximate relations have been obtained for a uniform mean flow in second-order stationary conductivity fields [see, e.g., *Dagan*, 1989; *Gelhar*, 1993]. Also, solute spreading for nonuniform flow [*Indelman and Rubin*, 1996] and in nonstationary conductivity fields (e.g., fields with evolving scales of heterogeneity [*Dagan*, 1994; *Neuman*, 1995; *Bellin et al.*, 1996]) has been investigated. The predicted solute spreading is related to the ensemble averaged concentrations obtained from many realizations of the hydraulic conductivity field. For a wide input source and a stationary conductivity field the ensemble average can be interchanged with the spatial average of concentrations in a single realization of the conductivity field. Often, the expected concentrations at a certain point in the aquifer are of interest. For some applications, however, we are interested to have the probability that a certain threshold concentration is exceeded. Therefore also the concentration variance has been approximated in second-order stationary conductivity fields. These approximations are derived either from a perturbation analysis of the convective-dispersive transport equation, referred to as the Eulerian approach [*Vomvoris and Gelhar*, 1990; *Kapoor and Gelhar*, 1994a; *Kapoor and Kitanidis*, 1996, 1998; *Andričević*, 1998], by a first-order analysis of the particle trajectories, the Lagrangian approach [e.g., *Dagan and Fiori*, 1997; *Pannone and Kitanidis*, 1999; *Fiori and Dagan*, 2000], or by a mixed Eulerian-Lagrangian approach [*Neuman*, 1995; *Zhang and Neuman*, 1996]. In contrast to the ensemble averaged concentrations, for which the Lagrangian and Eulerian approaches lead to the same predictions of the solute plume spreading, it is difficult to compare the two approaches for predicting concentration variances. First, the two approaches make different assumptions eventually leading to different predictions of the concentration variance, especially of the variance decay rate at large times (e.g., compare *Kapoor and Kitanidis* [1998] with *Fiori and Dagan* [2000]). Second, the Eulerian analysis points at the importance of the "microscale" of the hydraulic conductivity fluctu-

[1]Now at Institute of Chemistry and Dynamics of the Geosphere, Jülich, Germany.

Paper number 2001WR900009.
0043-1397/01/2001WR900009$09.00

ations which defines the expected value of the squared concentration perturbation gradients that acts as a sink term in the balance of the concentration variance. A derivation of the balance equation of the concentration variance [*Kapoor and Gelhar*, 1994a, Equation (9a)] is given in detail by *Kapoor and Gelhar* [1994a]. Since the microscale of the conductivity fields is only defined for differentiable conductivity fields, it remains unclear how the local concentration variances can be described for nondifferential conductivity fields, e.g., conductivity fields with an exponential spatial covariance, using an Eulerian approach.

The first-order approximations to predict ensemble averaged concentrations have been validated by numerical simulations of transport in heterogeneous conductivity fields [e.g., *Bellin et al.*, 1992; *Chin and Wang*, 1992; *Salandin and Fiorotto*, 1998; *Naff et al.*, 1998a, 1998b]. Numerical simulations to validate the approximations for the prediction of the concentration variances are relatively scarce [*Graham and McLaughlin*, 1989; *Burr et al.*, 1994; *Pannone and Kitanidis*, 1999] and are in some occasions used to calibrate rather than to validate the perturbation analyses [*Kapoor and Kitanidis*, 1998].

Besides the concentration variance, also the spatial covariance of local concentrations may be estimated using perturbation approximations. *Rubin* [1991] calculated spatial covariances of concentrations for purely advective transport from Monte Carlo simulations and suggested using them for conditioning concentration estimates on concentration measurements. Spatial covariances of solute arrival times to a reference surface have been estimated from the spatial covariance of the $\log_e$ transformed conductivity field in a Lagrangian framework for the case of advection dominated transport [*Rubin and Ezzedine*, 1997]. *Vanderborght and Vereecken* [2001] illustrated that predictions of the spatial covariance of solute arrival time using a first-order approximation of the particle trajectories were consistent with the spatial covariance of solute arrival times that was derived from local concentration measurements across the reference surface. This suggests that information on the spatial structure of local concentrations could be used to infer information on the spatial variability of the hydraulic conductivity field. Finally, the concentration variance dissipation due to dilution of the initially injected solute concentration can be used to estimate the local scale dispersion tensor [e.g., *Kapoor and Gelhar*, 1994b; *Andričević*, 1998; *Fiori and Dagan*, 1999].

In this paper, we will use a Lagrangian framework to approximate the variance and spatial covariance of local concentrations in heterogeneous, second-order stationary hydraulic conductivity fields. First, we will develop relations between the concentration covariance and the spatial covariance of the $\log_e$ transformed conductivity and the local scale dispersion using a method that follows more closely our understanding of the effect of local scale dispersion on the dilution of the injected solute concentration. Second, we will propose a methodology that simplifies the calculation of the concentration covariance for large injection volumes. Third, we will validate the concentration covariances based on a first-order approximation of the particle trajectories by concentration covariances that are derived from transport simulations in generated heterogeneous hydraulic conductivity fields. Finally, we will investigate how the parameters that characterize the spatial variability of the hydraulic conductivity and the local scale dispersion determine the spatial covariance of the concentration field. From this analysis we will identify parameters that can be derived unequivocally from the spatial covariance of local concentrations.

2. Perturbation Approximations

2.1. Particle Trajectory Statistics and Solute Concentrations

In this section, we will make the connection between the statistics of the particle trajectories and solute concentrations. We use the same Lagrangian framework as introduced by *Dagan* [1982] and later further developed by *Dagan and Fiori* [1997] and *Fiori and Dagan* [2000] to account for local scale dispersion on local solute concentrations. However, we suggest some modifications in the development of the relations between the particle trajectories and concentration in order to get a better perceptual understanding of this method. We must stress that our development does not lead to different relations as those obtained by *Dagan and Fiori* [1997] and *Fiori and Dagan* [2000], but it follows more closely the intuitive perception of solute transport in heterogeneous formations.

The Lagrangian framework can be considered as the limit of the particle tracking procedure in which first the trajectories of microscopic indivisible solute particles are calculated and subsequently the number of particles in an elementary volume at a certain time are counted to calculate the concentration distribution. Both the particle trajectories and elementary volumes are considered at the continuum or Darcy scale. Smaller-scale diffusion and dispersion processes are represented in the trajectory calculations by a Wiener process, which is the continuum limit of the random walk process. In former developments, the trajectory of a single fluid-solute particle, $\mathbf{X}(t; t_0, \mathbf{a})$, with a volume $\Delta\mathbf{a}$ that is initially centered around $\mathbf{a}$ in the injection volume, $\mathbf{V_0}$, was considered in a single realization of the Darcian velocity field. This leads to the following relation between the concentration field in a single realization of the Darcian velocity field and the trajectories of the Darcy scale fluid-solute particles:

$$C(\mathbf{x}, t) = \int_{V_0} C_0(\mathbf{a})\delta[\mathbf{x} - \mathbf{X}(t; t_0, \mathbf{a})]\, d\mathbf{a}. \qquad (1)$$

To obtain the average concentration distribution over all realizations of the Darcian velocity field and the Wiener process, one can start immediately from (1) and take the expectation of $C(\mathbf{x}, t)$ or $C^2(\mathbf{x}, t)$ and link it to the unconditional probability density distributions of one- and two-particle trajectories [*Pannone and Kitanidis*, 1999; *Fiori and Dagan*, 2000]. However, $C(\mathbf{x}, t)$ defined in (1) does not represent a measurable concentration since it suggests that even if local scale dispersion processes are included in the calculation of $\mathbf{X}(t; t_0, \mathbf{a})$ the initial concentration C_0 is not diluted, which contradicts the perception of the effect of local scale dispersion. In fact, this equation calculates the concentration field around a single, Darcian scale fluid-solute particle and represents the combined result of displacement in a single realization of the Darcian velocity field and of the Wiener process. However, the Wiener process represents velocity fluctuations at the sub Darcy scale whereas concentration measurements are made and initial concentrations, $C_0(\mathbf{a})$, are defined at the Darcy

scale in one realization of the Darcian velocity field. Therefore concentration measurements correspond with the macroscopic average of a large number of independent realizations of the Wiener process. These realizations represent the random displacements of a large number of indivisible solute particles that are defined at a microscopic scale and that reside at $t = t_0$ in the initial macroscopic solute-fluid body with volume $\Delta\mathbf{a}$. As a consequence, the concentration in a single realization of the Darcian velocity field is obtained from averaging the concentration fields around microscopic solute particles and it is related to the probability distribution of the trajectories of microscopic solute particles, which are conditioned on the Darcian velocity field. *Dagan and Fiori* [1997] followed this procedure but assumed that the variance of the conditioned microscopic solute particle trajectories depends only on the local scale dispersion process.

In the following, we will define $\Delta\mathbf{a}$ as an infinitesimal volume at the Darcy scale that is centered around $\mathbf{a}$ and in which the macroscopic variables: flow velocity, head, concentration, are constant. Since $\Delta\mathbf{a}$ is defined at the Darcy scale, it can contain a large number of indivisible and microscopic solute particles. Since $\Delta\mathbf{a}$ is infinitesimal at the Darcy scale with all Darcy scale variables constant within $\Delta\mathbf{a}$, all particles in $\Delta\mathbf{a}$ follow the same trajectory when transport is defined by velocities at the Darcy scale only, that is when local scale dispersion is not considered.

At $t = t_0$ we can relate the concentration in the injection volume to the number of particles, $n_0(\mathbf{a})$, in $\Delta\mathbf{a}$ centered around $\mathbf{a}$ as

$$\begin{aligned} C_0(\mathbf{a}, t_0) &= \lim_{\Delta a \to 0} [n_0(\mathbf{a}) dm/\Delta\mathbf{a}] && \mathbf{a} \in \mathbf{V_0} \\ C_0(\mathbf{a}, t_0) &= 0 && \mathbf{a} \notin \mathbf{V_0} \end{aligned} \tag{2}$$

with dm being the mass of a particle.

The concentration at a certain time t in an infinitesimal volume $\Delta\mathbf{x}$, which is centered around $\mathbf{x}$, is defined from the number of particles that reside in $\Delta\mathbf{x}$ at time t, $n(\mathbf{x}, t)$:

$$C(\mathbf{x}, t) = \lim_{\Delta x \to 0} [n(\mathbf{x}, t) dm/\Delta\mathbf{x}]. \tag{3}$$

In contrast to the approach of *Cvetkovic and Dagan* [1994], $\Delta\mathbf{a}$ and $\Delta\mathbf{x}$ in our development are not related to the volume of an indivisible solute-fluid particle. The volumes $\Delta\mathbf{a}$ and $\Delta\mathbf{x}$ are chosen to be equal by convention, and this equality does not stem from the Lagrangian statement of fluid continuity. The number of particles $n(\mathbf{x}, t)$ can be written as the number of particles, $n(\mathbf{x}, t; t_0, \mathbf{a})$, that started in $\Delta\mathbf{a}$ at $t = t_0$ and reach $\Delta\mathbf{x}$ at time t, summed up over all $\Delta\mathbf{a}$ in $\mathbf{V_0}$:

$$n(\mathbf{x}, t) = \sum_{all\ \Delta\mathbf{a}} n(\mathbf{x}, t; t_0, \mathbf{a}) = \frac{1}{\Delta\mathbf{a}} \int_{V_0} n(\mathbf{x}, t; t_0, \mathbf{a})\, d\mathbf{a}$$

$$= \frac{1}{\Delta\mathbf{a}} \int_{V_0} n_0(\mathbf{a}) P(\mathbf{x}, t; t_0, \mathbf{a})\, d\mathbf{a} \tag{4}$$

with $P(\mathbf{x}, t; t_0, \mathbf{a}) = n(\mathbf{x}, t; t_0, \mathbf{a})/n_0(\mathbf{a})$. For $n_0(\mathbf{a}) \to \infty$, $P(\mathbf{x}, t; t_0, \mathbf{a})$ corresponds with the probability that there is a particle trajectory $\mathbf{X}(t; t_0, \mathbf{a})$ in the given realization of the Darcian velocity field which reaches at time t the volume $\Delta\mathbf{x}$. Substitution of (3) in (4) and using (2) yields the following relation for $C(\mathbf{x}, t)$ in a single realization of the Darcian velocity field:

$$C(\mathbf{x}, t) = \lim_{\Delta x \to 0} \left(\frac{1}{\Delta\mathbf{x}} \int_{V_0} C_0(\mathbf{a}) P(\mathbf{x}, t; t_0, \mathbf{a})\, d\mathbf{a} \right)$$

$$= \int_{V_0} C_0(\mathbf{a}) \phi[\mathbf{x}; \mathbf{R}(t; t_0, \mathbf{a}), \Sigma(t; t_0, \mathbf{a})]\, d\mathbf{a} \tag{5}$$

with $\phi[\mathbf{x}; \mathbf{R}(t; t_0, \mathbf{a}), \Sigma(t; t_0, \mathbf{a})] = \lim_{\Delta x \to 0} [P(\mathbf{x}, t; t_0, \mathbf{a})/\Delta\mathbf{x}]$ the probability density function of particle trajectories $\mathbf{X}(t; \mathbf{a})$ at time t in a given realization of the Darcian velocity field. To simplify the notation, we set $t_0 = 0$ and skip it from the notation of probability density functions and their moments that are defined for the injection of particles at $t = t_0$. The probability density function $\phi[\mathbf{x}; \mathbf{R}(t; \mathbf{a}), \Sigma(t; \mathbf{a})]$ is characterized by the mean, $\mathbf{R}(t; \mathbf{a})$, and variance-covariance matrix, $\Sigma(t; \mathbf{a})$, of the coordinates of particle trajectories that start in a given realization of the Darcian velocity field in a volume $\Delta\mathbf{a}$. The concept of $\phi[\mathbf{x}; \mathbf{R}(t; \mathbf{a}), \Sigma(t; \mathbf{a})]$ is illustrated in Figure 1. The moments $\mathbf{R}(t; \mathbf{a})$ and $\Sigma(t; \mathbf{a})$ correspond with the center of mass and to the spreading of a plume which is injected in $\Delta\mathbf{a}$ in a specific realization of the Darcian velocity field. They are random variables with different values in different realizations of the Darcian velocity field. The spreading of a plume, which is injected in an infinitesimal injection volume, is caused by the combined effect of local scale dispersion and spatial variability of advection velocities and results in a dilution of the injected concentration, C_0. In Figure 2, locally injected plumes in heterogeneous and homogeneous flow fields are shown for different values of the local scale dispersion tensor. Plumes in the heterogeneous flow field are more diluted than in the homogeneous one due to the combined effect of local scale dispersion and advection velocity variability, which causes particles to move along different streamlines. In the Eulerian approach this larger dilution in a heterogeneous flow field is represented by the macrodispersive flux of the concentration variance in the concentration variance balance equation [*Kapoor and Gelhar*, 1994a]. In the following paragraph we relate the spreading of a locally injected plume, $\Sigma(t; \mathbf{a})$, to the spatial variability of the advection velocities and to the local scale dispersion tensor $\mathbf{D_d}$ using a Lagrangian framework.

To obtain the expected values of the concentration and the concentration variance, $C(\mathbf{x}, t)$ and $C^2(\mathbf{x}, t)$ must be averaged over all realizations of the random Darcian velocity field. If we assume that the largest part of the variability in $C(\mathbf{x}, t)$ between different realizations of Darcian velocity field stems from the variability in $\mathbf{R}(t; \mathbf{a})$, then $\Sigma(t; \mathbf{a})$ can be approximated by the ensemble average, that is, the expected value, $\langle\Sigma(t)\rangle$, and we obtain for the expected concentration:

$$\langle C(\mathbf{x}, t)\rangle = \int_{V_0} C_0(\mathbf{a}) \langle\phi[\mathbf{x}; \mathbf{R}(t; \mathbf{a}), \Sigma(t; \mathbf{a})]\rangle\, d\mathbf{a}$$

$$\approx \int \int_{V_0} C_0(\mathbf{a}) \phi[\mathbf{x} - \mathbf{R}(t; \mathbf{a}); \langle\Sigma(t; \mathbf{a})\rangle]$$

$$\cdot \Phi_{\mathbf{R}}[\mathbf{R}; t, \mathbf{a}]\, d\mathbf{a}\, d\mathbf{R} \tag{6}$$

and for the expected squared concentration:

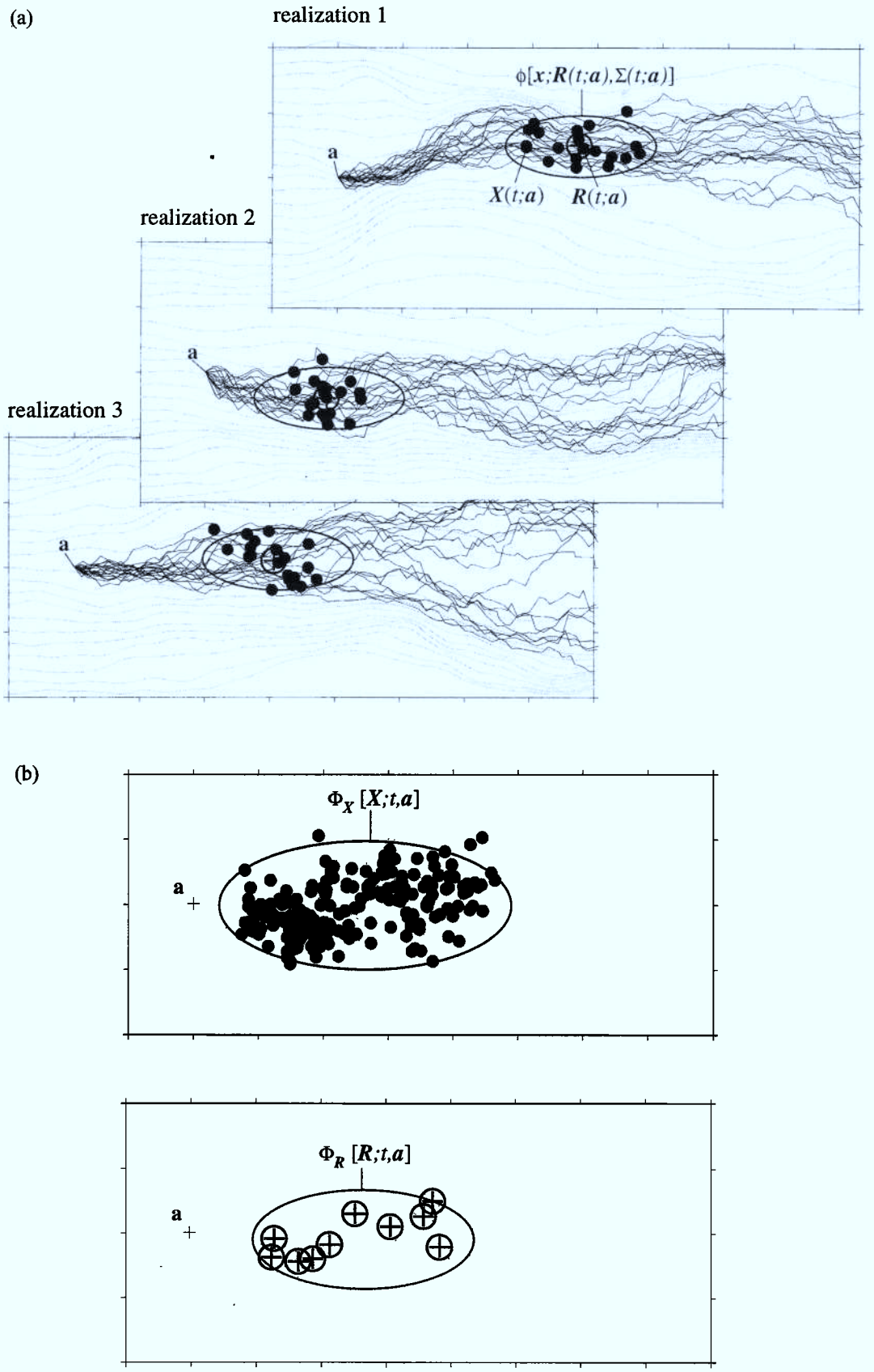

Figure 1. (a) Simulated advective and local scale dispersive trajectories of microscopic solute particles (black lines) that are released in an infinitesimal area $\Delta\mathbf{a}$ centered around $\mathbf{a}$ in a realization of the velocity field (gray lines represent flow lines), a schematic representation of the particle trajectory distribution, $\phi[\mathbf{x}; \mathbf{R}(t; \mathbf{a}), \Sigma(t; \mathbf{a})]$, and the centroïd of particle displacements, $\mathbf{R}(t; \mathbf{a})$ in one realization of the velocity field, and (b) a schematic representation of the trajectory, $\Phi_{\mathbf{X}}[t; \mathbf{a}]$, and centroïd, $\Phi_{\mathbf{R}}[t; \mathbf{a}]$ distributions in many realizations of the velocity field.

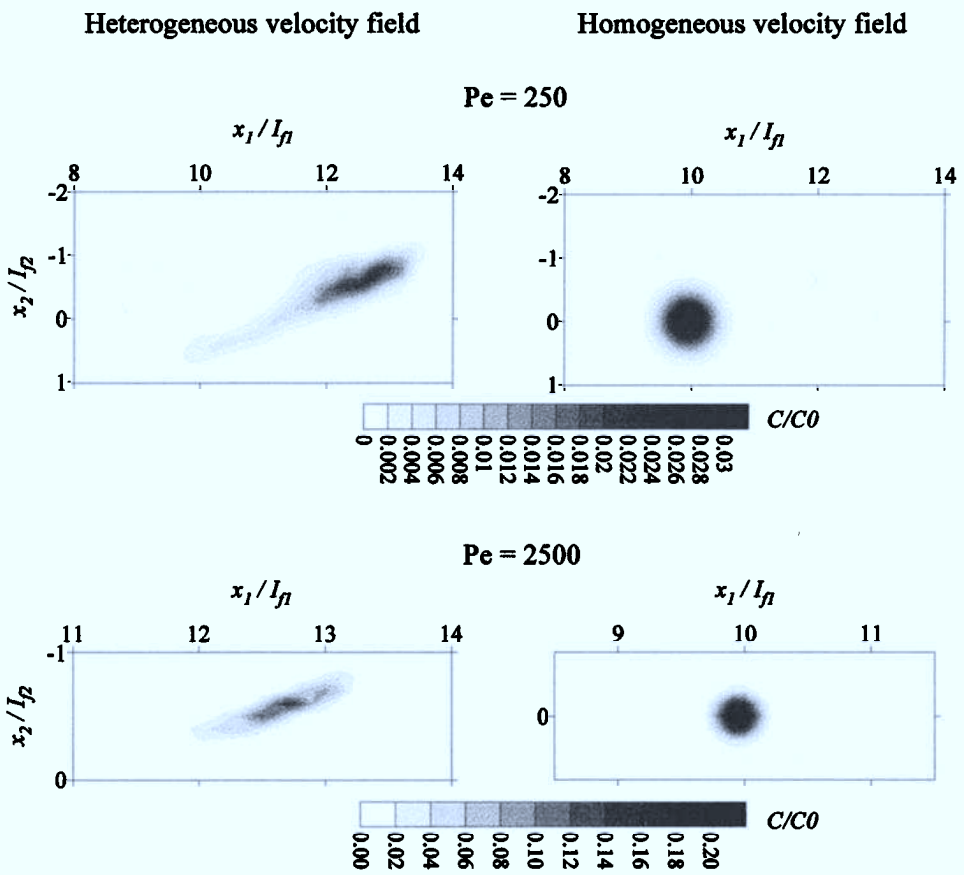

Figure 2. Simulated solute plumes in a heterogeneous and homogeneous velocity field at $t_n = tU/I_{f1} = 10$ for two different Peclet numbers ($Pe = UI_{f1}/D_d$). The heterogeneous velocity field was simulated in a heterogeneous 2-D conductivity field ($\sigma_f^2 = 0.5$ and $I_{f1} = I_{f2}$).

$$\langle C^2(\mathbf{x}, t)\rangle = \int_{V_0}\int_{V_0} C_0(\mathbf{a})C_0(\mathbf{b})\langle\phi[\mathbf{x}; \mathbf{R}(t; \mathbf{a}), \Sigma(t; \mathbf{a})] \cdot \phi[\mathbf{x}; \mathbf{S}(t; \mathbf{b}), \Sigma(t; \mathbf{b})]\rangle\, d\mathbf{a}\, d\mathbf{b}$$

$$\approx \int\int\int_{V_0}\int_{V_0} C_0(\mathbf{a})C_0(\mathbf{b})\phi[\mathbf{x} - \mathbf{R}(t; \mathbf{a}); \langle\Sigma(t)\rangle] \cdot \phi[\mathbf{x} - \mathbf{S}(t; \mathbf{b}); \langle\Sigma(t)\rangle]\Phi_{\mathbf{RS}}[\mathbf{R}, \mathbf{S}; t, \mathbf{a}, \mathbf{b}]\, d\mathbf{a}\, d\mathbf{b}\, d\mathbf{R}\, d\mathbf{S} \quad (7)$$

with $\mathbf{S}(t; \mathbf{b})$ the mean position at time t of particles that are injected in $\Delta\mathbf{b}$ in one realization of the Darcian velocity field, $\Phi_{\mathbf{R}}[\mathbf{R}; t, \mathbf{a}]$ the pdf of $\mathbf{R}(t; \mathbf{a})$, and $\Phi_{\mathbf{RS}}[\mathbf{R}, \mathbf{S}; t, \mathbf{a}, \mathbf{b}]$ the joint pdf of $\mathbf{R}(t; \mathbf{a})$ and $\mathbf{S}(t; \mathbf{b})$ in all realizations of the Darcian velocity field. The above equations can be rewritten in terms of the pdf, $\Phi_{\mathbf{X}}[\mathbf{X}; t, \mathbf{a}]$, and joint pdf, $\Phi_{\mathbf{XY}}[\mathbf{X}, \mathbf{Y}; t, \mathbf{a}, \mathbf{b}]$, of the particle trajectories $\mathbf{X}(t; \mathbf{a})$ and $\mathbf{Y}(t; \mathbf{b})$ (trajectory of another particle that is released in $\Delta\mathbf{b}$) in all realizations of the Darcian velocity field. A schematic illustration of the probability density functions, $\Phi_{\mathbf{R}}[\mathbf{R}; t, \mathbf{a}]$, $\Phi_{\mathbf{X}}[\mathbf{X}; t, \mathbf{a}]$ and $\phi[\mathbf{x}; \mathbf{R}(t; \mathbf{a}), \Sigma(t; \mathbf{a})]$ is given in Figure 1. The particle trajectory $\mathbf{X}(t; \mathbf{a})$ is split up as $\mathbf{X}(t; \mathbf{a}) = \tilde{\mathbf{X}}(t; \mathbf{a}) + \mathbf{R}(t; \mathbf{a})$, with $\tilde{\mathbf{X}}(t; \mathbf{a})$ a fluctuation around $\mathbf{R}(t; \mathbf{a})$ that is independent of $\mathbf{R}(t; \mathbf{a})$. From its definition it follows that the expected variance covariance matrix of $\tilde{\mathbf{X}}(t; \mathbf{a})$ is identical to $\langle\Sigma(t)\rangle$, the expected value of the variance covariance matrix of particle trajectory coordinates in a given realization of the Darcian velocity field. Hence the variance covariance matrix of the $\mathbf{X}(t; \mathbf{a})$ coordinates in all realizations of the Darcian velocity field, $\Xi(t) = \langle\Sigma(t)\rangle + \Sigma_{\mathbf{R}}(t)$ with $\Sigma_{\mathbf{R}}(t)$ the variance covariance matrix of the $\mathbf{R}(t; \mathbf{a})$ coordinates.

If we have a random variable $x = y + z$ with y and z independent random variables, then the pdf of x, $\text{pdf}_x(x)$, can be written in terms of the joint pdf of y and z, $\text{pdf}_{yz}(y, z)$ as

$$\text{pdf}_x(x) = \int \text{pdf}_{yz}(y = x - z, z)\, dz = \int \text{pdf}_y(x - z)\text{pdf}_z(z)\, dz. \quad (8)$$

Analogously, we have for the joint pdf, $\text{pdf}_{xx'}(x, x')$:

$$\text{pdf}_{xx'}(x, x') = \int\int \text{pdf}_{yy'zz'} \cdot (y = x - z, y' = x' - z', z, z')\, dz\, dz' = \int\int \text{pdf}_{yy'}(x - z, x' - z')\, \text{pdf}_{zz'}(z, z')\, dz\, dz'. \quad (9)$$

Making use of (8) and (9), we can write $\langle C(\mathbf{x}, t)\rangle$ and $\langle C^2(\mathbf{x}, t)\rangle$ in terms of the pdf $\Phi_{\mathbf{X}}[\mathbf{X}; t, \mathbf{a}]$, and the joint pdf

$\Phi_{XY}[\mathbf{X}, \mathbf{Y}; t, \mathbf{a}, \mathbf{b}]$ [*Pannone and Kitanidis*, 1999; *Fiori and Dagan*, 2000]:

$$\langle C(\mathbf{x}, t)\rangle = \int_{V_0} C_0(\mathbf{a})\Phi_{\mathbf{X}}[\mathbf{X} = \mathbf{x}; t, \mathbf{a}]\, d\mathbf{a} \tag{10}$$

$$\langle C^2(\mathbf{x}, t)\rangle = \int_{V_0}\int_{V_0} C_0(\mathbf{a})C_0(\mathbf{b})\Phi_{\mathbf{XY}}[\mathbf{X} = \mathbf{x}, \mathbf{Y} = \mathbf{x}; t, \mathbf{a}, \mathbf{b}]\, d\mathbf{a}\, d\mathbf{b}. \tag{11}$$

In our methodology we first look at the concentrations in one realization of the Darcian velocity field and link it to the probability distribution of microscopic particle trajectories in the specific Darcian velocity field. In a second step we average over all realizations of the Darcian velocity field. In this step we make the assumption that the spreading of a locally injected plume, which is characterized by the trajectory coordinate variance-covariance matrix, $\Sigma(t; \mathbf{a})$, is constant for all realizations of the Darcian velocity field and can be approximated by its ensemble average $\langle\Sigma(t)\rangle$. This approximation will lead to an underestimation of the concentration variances in all realizations of the Darcian velocity field since variability in $\Sigma(t; \mathbf{a})$ leads to an additional variability in $C(\mathbf{x}, t)$ with higher $C(\mathbf{x}, t)$ in realizations of the velocity field with a small $\Sigma(t; \mathbf{a})$ and vice versa for realizations with a high $\Sigma(t; \mathbf{a})$. Since our methodology finally leads to the same relationships as those that are obtained by averaging of (1) over different realizations of the Wiener process and of the Darcian velocity field, these approximations are also implicitly made when the other methodology is followed.

2.2. Variance and Covariance of the First-Order Approximated Trajectories of One and Two Particles

The variance of the first-order approximated particle trajectories, $X_{ij}(t)$ (ijth element of the variance covariance matrix $\Xi(t)$) is [*Dagan*, 1989]:

$$\frac{d^2X_{ij}(t)}{dt^2} \approx 4D_{dij}\delta(t) + 2\int_k \exp[i\mathbf{k}\cdot\mathbf{U}t - \mathbf{k}^{\mathrm{T}}\cdot\mathbf{D}_{\mathbf{d}}\cdot\mathbf{k}t]S_{uiuj}(\mathbf{k})\, d\mathbf{k} \tag{12}$$

with $\mathbf{k}$ the frequency vector, $\mathbf{D}_{\mathbf{d}}$ the local scale dispersion tensor, which is assumed to be constant, $\mathbf{U}$ the mean velocity vector, and $S_{uiuj}(\mathbf{k})$ the spectrum of the advection velocity fluctuations. In the sequel we consider the mean flow in the x_1 direction ($\mathbf{U} = (U, 0, 0)$) and a diagonal local scale dispersion tensor with $D_{d11} = D_L$ and $D_{d,ii}$ $(i \neq 1) = D_T$. Integration over time yields

$$X_{ij}(t) \approx 2D_{d,ij}\, t + 2\int_k \left\{\{-(D_{dpp}k_p^2)^2 + k_1^2U^2 + \exp(-D_{dpp}k_p^2\, t)[\cos(k_1Ut)((D_{dpp}k_p^2)^2 - k_1^2U^2) - 2k_1U\sin(k_1U\, t)\, D_{dpp}k_p^2]\}((D_{dpp}k_p^2)^2 + k_1^2U^2)^{-2} + \frac{D_{dpp}k_p^2 t}{(D_{dpp}k_p^2)^2 + k_1^2U^2}\right\} S_{uiuj}(\mathbf{k})\, d\mathbf{k} \tag{13}$$

with the index p referring to a summation over the different coordinates.

The covariance between the first-order approximated trajectories of two particles $\mathbf{X}(t; \mathbf{a})$ and $\mathbf{Y}(t; \mathbf{b})$, $Z_{ij}(t; \mathbf{a}, \mathbf{b}) = \langle(\mathbf{X}(t; \mathbf{a}) - \langle\mathbf{X}(t; \mathbf{a})\rangle)(\mathbf{Y}(t; \mathbf{b}) - \langle\mathbf{Y}(t; \mathbf{b})\rangle)\rangle = \langle\hat{\mathbf{X}}(t; \mathbf{a})\hat{\mathbf{Y}}(t; \mathbf{b})\rangle$, is derived as [*Fiori and Dagan*, 1999, 2000]:

$$\frac{\partial^2\langle\hat{X}_i(t; \mathbf{a})\hat{Y}_j(t'; \mathbf{b})\rangle}{\partial t\partial t'} = \langle u_i[\mathbf{X}(t; \mathbf{a})]u_j[\mathbf{Y}(t; \mathbf{b})]\rangle \approx \int_k \exp[i\mathbf{k}\cdot(\mathbf{U}t - \mathbf{U}t' + \mathbf{a} - \mathbf{b}) - \mathbf{k}^{\mathrm{T}}\cdot\mathbf{D}_{\mathbf{d}}\cdot\mathbf{k}(t + t')]S_{uiuj}(\mathbf{k})\, d\mathbf{k}. \tag{14}$$

Integration over t and t' yields

$$Z_{ij}(t; \mathbf{a}, \mathbf{b}) = Z_{ij}(t; \mathbf{a} - \mathbf{b}) \approx \int_k [1 - 2\cos(k_1Ut)\exp(-k_p^2D_{dpp}t) + \exp(-2k_p^2D_{dpp}t)]\cos[(k_p(a_p - b_p)] \cdot [(D_{dpp}k_p^2)^2 + k_1^2U^2]^{-1} S_{uiuj}(\mathbf{k})\, d\mathbf{k} \tag{15}$$

In Appendix A, $X_{ij}(t)$ and $Z_{ij}(t; \mathbf{a} - \mathbf{b})$ are written in terms of dimensionless variables for two-dimensional (2-D) flow and for an exponential spatial covariance of the $\log_e$ transformed conductivities. A more general set of solutions of (13) and (15) is given by *Fiori* [1996] and *Fiori and Dagan* [2000].

The ijth element of the variance-covariance matrix of $\mathbf{R}(t; \mathbf{a})$, $\Sigma_{\mathbf{R}}(t)$, is equal to the two particle covariance $Z_{ij}(t; \mathbf{a}, \mathbf{a})$:

$$\begin{aligned}\Sigma_{\mathbf{R}}(t) &= \langle(R_i(t; \mathbf{a}) - \langle R_i(t; \mathbf{a})\rangle)(R_j(t; \mathbf{a}) - \langle R_j(t; \mathbf{a})\rangle)\rangle \\ &= \langle\hat{R}_i(t; \mathbf{a})\hat{R}_j(t; \mathbf{a})\rangle \\ &= \lim_{\Delta a\to 0}\left(\frac{1}{\Delta\mathbf{a}^2}\int_{\Delta\mathbf{a}}\int_{\Delta\mathbf{a}}\langle\hat{X}_i(t; \mathbf{a})\hat{Y}_j(t; \mathbf{a}')\rangle\, d\mathbf{a}\, d\mathbf{a}'\right) \\ &= \lim_{\Delta a\to 0}\left(\frac{1}{\Delta\mathbf{a}^2}\int_{\Delta\mathbf{a}}\int_{\Delta\mathbf{a}} Z_{ij}(t; \mathbf{a}, \mathbf{a}')\, d\mathbf{a}\, d\mathbf{a}'\right) \\ &= Z_{ij}(t; \mathbf{a}, \mathbf{a})\end{aligned} \tag{16}$$

As a consequence, the ijth element of the expected value of the spreading of a locally injected plume, $\langle\Sigma(t)\rangle$, is obtained form the particle trajectory variance and two particle trajectory covariance as

$$\langle\Sigma_{ij}(t)\rangle = X_{ij}(t) - Z_{ij}(t; \mathbf{a}, \mathbf{a}). \tag{17}$$

2.3. Concentration Variance and Spatial Covariance for Large Injection Volumes

To calculate $\langle C^2(\mathbf{x}, t)\rangle$, one needs to evaluate (11) which involves six (3-D flow) or four (2-D flow) quadratures. For each value of $\mathbf{a}$ and $\mathbf{b}$ the two particle covariance, $Z_{ij}(t; \mathbf{a}, \mathbf{b})$, needs to be calculated. To simplify the calculation of (11), *Dagan and Fiori* [1997] and *Fiori and Dagan* [2000] considered small injection surfaces $\mathbf{V_0}$ in which $Z_{ij}(t; \mathbf{a}, \mathbf{b}) = Z_{ij}(t; \mathbf{a} - \mathbf{b}) \approx Z_{ij}(t; \mathbf{0})$.

However, (11) can also be dramatically simplified if one

considers the "backward" particle trajectories, $\mathbf{A}(t'; t, \mathbf{x})$. A similar approach was used by *Rubin and Ezzedine* [1997] and *Vanderborght and Vereecken* [2001] to analyze the spatial correlation of solute arrival time to a reference surface and by *Dagan et al.* [1996] to condition aquifer conductivity on particle trajectories. The backward particle trajectory, $\mathbf{A}(t'; t, \mathbf{x})$, represents the location at a time t' of a fictitious particle that reaches $\Delta\mathbf{x}$ centered around $\mathbf{x}$ at time t. The number of particles in $\Delta\mathbf{x}$ around $\mathbf{x}$ at time t, $n(\mathbf{x}, t)$, can be expressed in terms of the number of fictitious particles of which the 'backward' trajectory at time $t = t_0$ was in the injection volume $\mathbf{V_0}$: $n^f(\mathbf{A} = \mathbf{a} \in \mathbf{V_0}, t_0; t, \mathbf{x})$, which is, in turn, related to the probability density function of $\mathbf{A}(t' = t_0; t, \mathbf{x})$:

$$n(\mathbf{x}, t) = \sum_{all\ \Delta\mathbf{a}} \frac{n_0(\mathbf{a}) n^f(\mathbf{A} = \mathbf{a}, t_0; t, \mathbf{x})}{n_0^f(\mathbf{x})}$$

$$= \frac{1}{\Delta\mathbf{a}} \int_{V_0} \frac{n_0(\mathbf{a}) n^f(\mathbf{A} = \mathbf{a}, t_0; t, \mathbf{x})}{n_0^f(\mathbf{x})} d\mathbf{a}$$

$$= \frac{1}{\Delta\mathbf{a}} \int_{V_0} n_0(\mathbf{a}) P(\mathbf{A} = \mathbf{a}, t_0; t, \mathbf{x})\, d\mathbf{a} \qquad (18)$$

with $n_0^f(\mathbf{x})$ the number of fictitious particles that reach $\Delta\mathbf{x}$ at time t, and $P(\mathbf{A} = \mathbf{a}, t_0; t, \mathbf{x})$ the probability that in a given realization of the Darcian velocity field, the backward trajectory of a fictitious particle, which reaches $\Delta\mathbf{x}$ at time t, was at time $t' = t_0$ in $\Delta\mathbf{a}$. Dividing first both sides of (18) by $\Delta\mathbf{x}$ and subsequently making use of the convention $\Delta\mathbf{x} = \Delta\mathbf{a}$ to replace $\Delta\mathbf{x}$ in the right-hand side of (18) by $\Delta\mathbf{a}$, yields

$$C(\mathbf{x}, t) = \int_{V_0} C_0(\mathbf{a}) \phi_{\mathbf{A}}[\mathbf{A} = \mathbf{a}; \mathbf{R_A}(t_0; t, \mathbf{x}), \mathbf{\Sigma_A}(t_0)]\, d\mathbf{a} \qquad (19)$$

with $\phi_{\mathbf{A}}[\mathbf{A} = \mathbf{a}; \mathbf{R_A}(t_0; t, \mathbf{x}), \mathbf{\Sigma_A}(t_0)] = \lim_{\Delta a \to 0} [P(\mathbf{A} = \mathbf{a}, t_0; t, \mathbf{x})/\Delta\mathbf{a}]$ the probability density function and $\mathbf{R_A}(t_0; t, \mathbf{x})$ and $\mathbf{\Sigma_A}(t_0)$ the mean and variance of the backward trajectory $\mathbf{A}(t' = t_0; t, \mathbf{x})$ in a given realization of the Darcian velocity field. Similarly, as for the "forward" trajectories, we obtain after averaging over different realizations of the Darcian velocity field:

$$\langle C(\mathbf{x}, t) \rangle = \int_{V_0} C_0(\mathbf{a}) \Phi_{\mathbf{A}}[\mathbf{A} = \mathbf{a}; t, \mathbf{x}]\, d\mathbf{a} \qquad (20)$$

$$\langle C^2(\mathbf{x}, t) \rangle = \int_{V_0} \int_{V_0} C_0(\mathbf{a}) C_0(\mathbf{b}) \cdot \Phi_{\mathbf{AB}}[\mathbf{A} = \mathbf{a}, \mathbf{B} = \mathbf{b}; t, \mathbf{x}, \mathbf{x}]\, d\mathbf{a}\, d\mathbf{b} \qquad (21)$$

with $\mathbf{\Phi_A}[\mathbf{A}; t, \mathbf{x}]$ and $\mathbf{\Phi_{AB}}[\mathbf{A}, \mathbf{B}; t, \mathbf{x}, \mathbf{y}]$ the one and two particle backward trajectory pdfs in all realizations of the Darcian velocity field at time t_0. The moments of the backward trajectory pdf's, $X_{ij}(t_0 - t)$ and $Z_{ij}(t_0 - t; \mathbf{x}, \mathbf{x})$, are obtained using the same equations as those for the forward trajectories (equations (13) and (15)). Using the backward trajectory pdf's simplifies the calculation of the concentration variance in two ways. First, the two particle covariance $Z_{ij}(t_0 - t; \mathbf{x}, \mathbf{x})$ must be calculated only for the separation $\mathbf{x} - \mathbf{x} = \mathbf{0}$. Second, since the probability density function is integrated in (21) over the random variables $\mathbf{a}$ and $\mathbf{b}$, the integration simplifies for large injection volumes whereby random variables are integrated out. If we consider a uniform concentration in the injection volume and an injection volume $\mathbf{V_0} = (L_1, L_2, L_3)$, which is a thin slab perpendicular to the mean flow direction with $L_1 \ll I_{f1}$, and $L_{2,3} \gg I_{f2,f3}$, the variables a_2, a_3, b_2, and b_3 are integrated out and (21) simplifies to

$$\langle C^2(\mathbf{x}, t) \rangle = C_0^2 \int_{L_1} \int_{L_1} \Phi_{A1B1}[A_1 = a_1, B_1 = b_1; t, \mathbf{x}, \mathbf{x}]\, da_1\, db_1$$

$$\approx C_0^2 L_1^2 \Phi_{A1B1}[A_1 = 0, B_1 = 0; t, \mathbf{x}, \mathbf{x}]. \qquad (22)$$

Equation (22) can be extended to calculate the concentration spatial covariance: $C_{CC}(\mathbf{x}, \mathbf{y}; t) = \langle C(\mathbf{x}, t) C(\mathbf{y}, t) \rangle - \langle C(\mathbf{x}, t) \rangle \langle C(\mathbf{y}, t) \rangle$ with:

$$\langle C(\mathbf{x}, t) C(\mathbf{y}, t) \rangle \approx C_0^2 L_1^2 \Phi_{A1B1}[A_1 = 0, B_1 = 0; t, \mathbf{x}, \mathbf{y}]. \qquad (23)$$

Since for stationary conductivity fields and a uniform mean flow $Z_{11}(t; \mathbf{x}, \mathbf{y}) = Z_{11}(t; \mathbf{x} - \mathbf{y}, \mathbf{0})$, $\Phi_{A1B1}[A_1 = 0, B_1 = 0; t, \mathbf{x}, \mathbf{y}]$ equals $\Phi_{A1B1}[A_1 = 0, B_1 = 0; t, (x_1, x_2 - y_2, x_3 - y_3), (y_1, 0, 0)]$ and $C_{CC}(\mathbf{x}, \mathbf{y}; t)$ is for a large lateral extent of $\mathbf{V_0}$ invariant to translations in the transverse to flow direction. As a consequence, $C_{CC}(\mathbf{x}, \mathbf{y}; t)$ can be derived from concentration measurements in a single realization of the conductivity field.

3. Numerical Transport Simulations

To validate the first-order approximations, we carried out numerical simulations of solute transport in generated heterogeneous conductivity fields. Because of computational limitations, the simulations were carried out in two-dimensional conductivity fields. Although quantitatively different from transport in three-dimensional media, the 2-D flow and transport simulations can be used to evaluate the first-order approximations. The conductivity fields were generated by a spectral random field generator [*Gutjahr et al.*, 1995]. In all fields the spatial covariance of the $\log_e$ transformed conductivity fluctuations f was modeled by an exponential spatial covariance function:

$$C_{ff}(\mathbf{x}) = \sigma_f^2 \exp\left(- \sqrt{\left(\frac{x_1}{I_{f1}}\right)^2 + \left(\frac{x_2}{I_{f2}}\right)^2} \right) \qquad (24)$$

with σ_f^2 the variance of the $\log_e$ transformed conductivity and I_{fi} the spatial correlation length of f in direction i. Three types of conductivity fields were considered: an isotropic ($I_{f1} = I_{f2}$), and two anisotropic fields: $I_{f1} = 2\, I_{f2}$ (anisotropic field 1) and $I_{f1} = 0.5\, I_{f2}$ (anisotropic field 2). The correlation length in the x_2 direction (transverse to flow direction) was constant for the three conductivity fields. For the three field types, conductivities were generated on a square grid of 512 × 512 nodes with 10 nodes per correlation length I_{f2} in the x_2 direction. For the isotropic field this discretization resulted in 10 nodes per correlation length I_{f1}, whereas the discretization was, respectively, 20 and 5 nodes per correlation length I_{f1} for

the anisotropic fields 1 and 2. The variance σ_f^2 was chosen to be 0.5 for the isotropic field. For the anisotropic fields, σ_f^2 was chosen so that first-order estimate of the spreading of the plumes in the mean flow direction, $X_{11}(t)$, after having traveled over a distance 5 I_{f2} (= 5 I_{f1} for the isotropic field, 2.5 I_{f1} for the anisotropic field 1, and 10 I_{f1} for anisotropic field 2) was the same in the three conductivity fields. The corresponding σ_f^2 was 0.2863 and 0.9499 for anisotropic fields 1 and 2, respectively.

To avoid periodicity in the generated conductivity fields, flow and transport were simulated in subdomains of 200 × 200 nodes that were selected from the generated 512 × 512 fields. Flow was simulated using the SWMS_2D code [*Šimůnek et al.*, 1994], which solves Darcy flow equation using the Galerkin finite element method. Mean flow in the x_1 direction was driven by a mean unit gradient with a constant head applied at the inlet and outlet of the flow domain. No-flow boundaries were defined at the lateral boundaries of the flow domain. Solute transport was simulated using a particle tracking scheme similar to the one used by *Roth and Hammel* [1996]. The fourth-order Runge-Kutta method was used to solve the particle displacement by advection during a discrete time step Δt. The discrete time step Δt was adapted so that the space step was smaller than 0.5 Δx_1 (the grid size). Local scale dispersion was modeled by adding a random displacement $\Delta \mathbf{x}_d$ to the advective displacement. The variance tensor of the random variable $\Delta \mathbf{x}_d$ was defined by the local scale dispersion tensor, $\mathbf{D}_d$ and the time step Δt:

$$\Sigma_{\Delta xd} = 2\mathbf{D}_d \Delta t. \tag{25}$$

Simulations were done for four different values of the local scale dispersion, which was assumed to be isotropic ($D_{dij} = 0$ for $i \neq j$; $D_{d11} = D_{d22}$) and constant in space. The corresponding Peclet numbers ($Pe_T = UI_{f2}/D_{d11}$) were 25, 250, 2500, and infinity. Note that we define the Peclet number in terms of correlation scale in direction transverse to the mean flow, I_{f2}. As will be illustrated further, this definition is more directly related to the concentration variance dissipation due to local scale dispersion than a Peclet number defined in terms of the correlation scale of the hydraulic conductivity in the mean flow direction, I_{f1}. In a first set of simulations the trajectories of 242 particles that were released at regular intervals (0.1 I_{f2}) along a line perpendicular to the mean flow direction, with two particles released at each location, were simulated in 200 realizations of the isotropic conductivity field to evaluate the first-order approximations of the two particle trajectory covariance, $Z_{ij}(t; \mathbf{a} - \mathbf{b})$. The injection line was positioned at 4 I_{f2} from the lateral domain boundary and at 2 I_{f1} from the uniform head boundary at the flow inlet.

In a second set of simulations, solute concentration plumes were simulated in 10 realizations of the isotropic and of the two anisotropic conductivity fields. In each realization of the conductivity field, 500,000 particles were injected uniformly in a slab with a length of $L_2 = 16\ I_{f2}$ and a width of $L_1 = 0.2\ I_{f2}$. The slab was positioned perpendicular to the mean flow direction at a distance $2I_{f2}$ from the lateral boundaries and a distance $2I_{f2}$ from the constant head boundary at the flow inlet. The concentration profiles were determined from counting the number of particles in each square grid cell at preset times. Average concentration profiles and the variance of local concentration along a transect transverse to the mean flow direction were also calculated for a larger number of injected particles (2×10^6) but were not significantly different from concentration profiles and concentration simulated with a smaller amount of particles.

Since we chose an exponential spatial covariance model, we considered hydraulic conductivity fields that are not differentiable. However, the numerical solution of the flow equation smooths out conductivity fluctuations over the elements of the numerical grid and filters out the high frequency components of the conductivity fluctuations. Neglecting high-frequency components of the conductivity fluctuations leads to an underestimation of small-scale advective velocity fluctuations. For large Peclet numbers, neglecting these small-scale fluctuations reduces the particle trajectory variance, $X_{ii}(t)$, more than the two particle trajectory covariance, $Z_{ii}(t, \mathbf{0})$, since small-scale velocity fluctuations are filtered from the trajectory covariance by local scale dispersion. Therefore neglecting small-scale velocity fluctuations results in a larger underestimation of $X_{ii}(t)$ than of $Z_{ii}(t, \mathbf{0})$, which leads to an overestimation of the concentration variance. On the other hand, averaging concentrations over a grid element smooths out local concentration fluctuations and reduces the simulated concentration variance. To evaluate these effects on the numerically simulated concentration variances, we simulated flow and transport for the same initial and boundary conditions as defined above in one realization of the isotropic conductivity field using two discretizations: $\Delta x_1 = \Delta x_2 = 0.05\ I_{f1}$ ("fine" discretization) and $\Delta x_1 = \Delta_{x2} = 0.1\ I_{f1}$ ("coarse" discretization). To distinguish the effects of smoothing out the conductivity field, which increases in the concentration variance, and smoothing out the concentration field, which decreases the concentration variance, concentration variances were also calculated from averaged concentrations that were simulated with a fine discretization. In Table 1a the concentration variance along a line perpendicular to the mean flow direction and integrated across the direction of the mean flow is shown for the different discretization scenarios. The integrated concentration variances were normalized versus the concentration variance for the fine grid simulations. Note in Table 1a. (1) the compensating effect of smoothing the conductivity and the concentration fields on the simulated concentration variance, and (2) the relatively small difference in concentration variances for the different discretization scenarios indicating that the simulations using the coarser discretization reproduce the concentration variances fairly well. The effect of smoothing the conductivity and the concentration over the scale of the grid elements on the numerically simulated concentration variance can also be estimated using a first-order approximation. The power spectrum of the averaged conductivities is derived from the original conductivity power spectrum and used to calculate the moments of the particle trajectory distributions (equation (13) and (15)) which are subsequently used to calculate the concentration spatial covariance (equations (22) and (23)). Using the approximation of the concentration covariance, the variance of averaged concentrations over the grid elements is derived. In Table 1b, approximate concentration variances for different relative grid sizes: $\Delta x_i/I_{fi}$, are listed.

4. Results

4.1. Two-Particle Trajectory Distribution and Covariance: $Z_{ij}(t; \mathbf{a} - \mathbf{b})$

Since the concentration variance is defined by the two particle trajectory pdf, $\Phi_{\mathbf{XY}}[\mathbf{X}, \mathbf{Y}; t, \mathbf{a} - \mathbf{b}]$ (equation (11)) or $\Phi_{\mathbf{AB}}[\mathbf{A}, \mathbf{B}; t_0, \mathbf{x}, \mathbf{x}]$ (equation (21)), we first check whether the

Table 1a. Effect of the Numerical Grid Δx on the Simulated Concentration Variance Along a Line Transverse to the Flow Direction for an Initially Wide Injection Volume and in a Heterogeneous Conductivity Field With an Exponential Spatial Covariance for Numerically Simulated Concentration Variance in One Realization of the Conductivity Field (Concentration Variances Are Integrated Along the Main Flow Direction $\|\sigma_C^2|_n$)

		t_n[a]			
Δx_n[b] (Flow)	Δx_n (Transport)	1.25	2.5	5	10
		Pe[c] = 2500			
0.05	0.05	1.000[d]	1.000	1.000	1.000
0.1	0.05	1.032	1.034	1.044	1.050
0.05	0.1	0.859	0.883	0.903	0.941
0.1	0.1	0.895	0.909	0.940	0.984
		Pe = 250			
0.05	0.05	1.000	1.000	1.000	1.000
0.1	0.05	1.023	1.022	1.019	1.023
0.05	0.1	0.951	0.971	0.980	0.986
0.1	0.1	0.971	0.989	0.998	1.007
		Pe = 25			
0.05	0.05	1.000	1.000	1.000	1.000
0.1	0.05	1.000	1.006	1.004	1.011
0.05	0.1	0.984	0.988	0.987	0.982
0.1	0.1	0.984	0.994	0.991	0.993

[a] $t_n = tU/I_{f1}$.
[b] $\Delta x_n = \Delta x/I_{f1}$.
[c] $Pe = UI_{f1}/D_d$.
[d] Concentration variances are normalized versus the variance for the finest numerical grid.

multivariate pdf can be approximated by a multivariate Gaussian or normal pdf. For $\mathbf{a} - \mathbf{b} = (a_1 - b_1, 0)$ or $\mathbf{a} - \mathbf{b} = (0, a_2 - b_2)$ the first order approximation of $Z_{ij}(t; \mathbf{a} - \mathbf{b}) = 0$ for $i \neq j$ and $\Phi_{\mathbf{XY}}[\mathbf{X}, \mathbf{Y}; t, \mathbf{a} - \mathbf{b}] = \Phi_{X1Y1}[X_1, Y_1; t, \mathbf{a} - \mathbf{b}]\Phi_{X2Y2}[X_2, Y_2; t, \mathbf{a} - \mathbf{b}]$. The normality of the bivariate pdfs

Table 1b. Same as Table 1a but for First-Order Approximation of the Concentration Variance at the Center of the Plume σ_{cp}^2[a] Concentration Variances Are Normalized Versus the Variance for the Finest Numerical Grid

Δx_n (Flow and Transport)	t_n		
	2.5	5	10
	Pe = 2500		
−>0	1.000	1.000	1.000
0.025	0.967	0.984	0.992
0.050	0.897	0.942	0.971
0.100	0.748	0.834	0.903
0.200	0.539	0.657	0.762
	Pe = 250		
−>0	1.000	1.000	1.000
0.025	0.997	0.999	0.999
0.050	0.989	0.995	0.999
0.100	0.959	0.982	0.995
0.200	0.866	0.931	0.974
	Pe = 25		
−>0	1.000	1.000	1.000
0.025	1.000	1.000	1.000
0.050	0.999	1.000	1.001
0.100	0.995	1.000	1.003
0.200	0.977	0.998	1.008

[a] Concentration variances are normalized versus the variance for the finest numerical grid.
[b] $t_n = tU/I_{f1}$.
[c] $\Delta x_n = \Delta x/I_{f1}$.
[d] $Pe = UI_{f1}/D_d$.

$\Phi_{X1Y1}[X_1, Y_1; t, \mathbf{a} - \mathbf{b}]$ and $\Phi_{X2Y2}[X_2, Y_2; t, \mathbf{a} - \mathbf{b}]$ was evaluated from the distribution of the Mahalanobis distances, m^2, of the pairs (X_1, Y_1) and (X_2, Y_2). The Mahalanobis distance is defined as [*Jobson*, 1992]

$$m^2 = \frac{1}{1 - \dfrac{Z_{ii}^2(t; \mathbf{a} - \mathbf{b})}{X_{ii}^2(t)}} [(X_i - \langle X_i \rangle)^2 + (Y_i - \langle Y_i \rangle)^2 - \{2 [Z_{ii}(t; \mathbf{a} - \mathbf{b})/X_{ii}(t)]\} \cdot (X_i - \langle X_i \rangle)(Y_i - \langle Y_i \rangle)]/[X_{ii}(t)]. \quad (26)$$

The ordered Mahalanobis distances, $m_{(i)}^2$, $i = 1, 2, \ldots, n$, with n the number of pairs (X_i, Y_i), can be compared with the χ^2 distribution, $\chi_{(1-\alpha i);2}^2$ with $\alpha_i = (i - 0.5)/n$. For a bivariate normal distribution a plot of the points $(m_{(i)}^2, \chi_{(1-\alpha i);2}^2)$ should yield a straight line. In Figure 3 the Mahalanobis distances of the pairs (X_1, Y_1) and (X_2, Y_2), which were simulated in 200 realizations of the isotropic conductivity field for $\sigma_f^2 = 0.5$, $Pe = \infty$, and $\mathbf{a} - \mathbf{b} = (0, I_{f2})$, are plotted versus $\chi_{(1-\alpha i);2}^2$. The distribution of the pairs of particle trajectories coordinates in the mean flow direction, (X_1, Y_1), follows fairly closely a bivariate normal distribution whereas the distribution of the pairs (X_2, Y_2) of the transverse particle trajectory coordinates apparently has a higher kurtosis. This finding is in line with previous analyses of the univariate distributions of particle trajectory coordinates [e.g., *Salandin and Fiorotto*, 1998].

In Figure 4 the first-order approximated two particle trajectory covariances, $Z_{ii}(t; \mathbf{a} - \mathbf{b})$ (equation (15)) and covariances derived from particle tracking simulations in the isotropic conductivity field ($\sigma_f^2 = 0.5$, $Pe = \infty$), are plotted versus the initial separation of the two particles: $(0, a_2 - b_2)$. The transverse displacements of two different particles remain positively correlated for a larger range of transverse separation of the initial

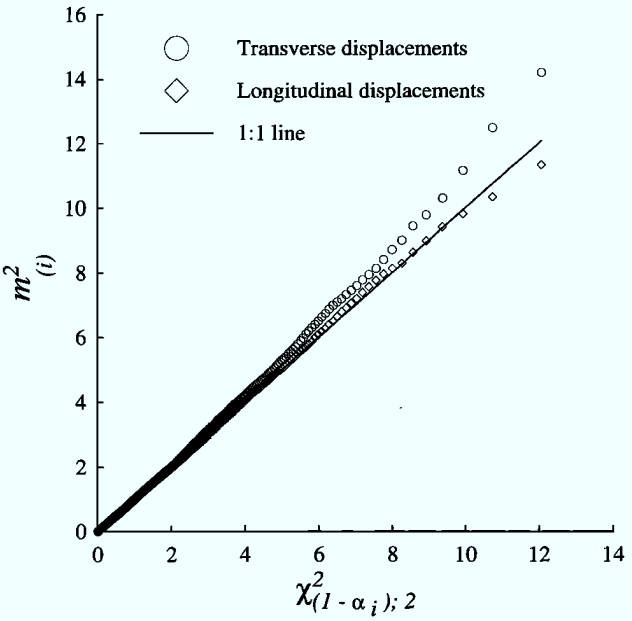

Figure 3. Ordered Mahalanobis distances, $m^2_{(i)}$, of pairs of longitudinal (X_1, Y_1) and transverse (X_2, Y_2) advective ($Pe = UI_{f1}/D_d = \infty$) displacements of two particles with an initial separation $\mathbf{a} - \mathbf{b} = (0, I_{f2})$ in a 2-D conductivity field with $\sigma_f^2 = 0.5$ and $I_{f1} = I_{f2}$ at $t_n = tU/I_{f1} = 10$ after injection versus the percentiles of the χ^2 distribution.

particle locations than the longitudinal particle displacements in the mean flow direction. For both the transverse and longi tudinal particle displacements the first-order approximation underestimates the covariance, especially for larger separation distances $(0, a_2 - b_2)$. Local scale dispersion decreases the trajectory covariances for relatively small initial separation distances of the two particles. The effect of local scale dispersion on the trajectory covariances is relatively well reproduced by the first-order approximations of the particle trajectories. For the estimation of the concentration variance using (22) the correlation of particle trajectories, $Z_{ii}(t; \mathbf{0})/X_{ii}(t)$, is of importance. Since the variance of the particle trajectories is also underestimated by the first-order approximations, the correlation of particle trajectories is well reproduced by the first-order approximations (see Figure 5) for relatively small initial separation distances.

4.2. Mean and Standard Deviation of Local Concentrations in Isotropic Conductivity Fields

In Figure 6, concentration profiles of averaged concentrations, $\langle C(x_1, t)\rangle$, along lines perpendicular to the mean flow direction in the 10 realizations of the generated isotropic conductivity fields are shown together with the standard deviation of the local concentration along these lines, $\sigma_C(x_1, t)$. Results are shown for simulations with $Pe = 250$ when the plume has traveled over a distance 2.5 I_{f1}, 5 I_{f1} and 10 I_{f1} and for simulations with **Pe** = 25 and $Pe = 2500$ when the plume has traveled over a distance 5 I_{f1}. Also shown are first-order predictions of $\langle C(x_1, t)\rangle$ and $\sigma_C(x_1, t)$. The approximation of the average concentration, $\langle C(x_1, t)\rangle$, for small L_1 was calculated assuming a normal distribution of longitudinal particle locations:

$$\langle C(x_1, t)\rangle = \frac{L_1 C_0}{\sqrt{2\pi X_{11}(t)}} \exp\left(-\frac{1}{2}\frac{(x_1 - Ut)^2}{X_{11}(t)}\right). \quad (27)$$

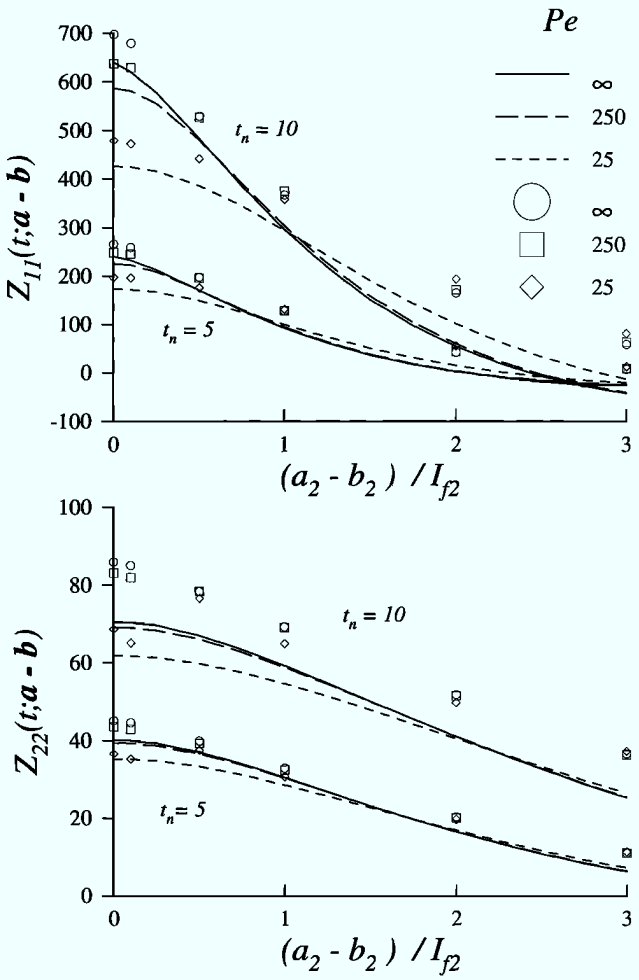

Figure 4. Covariance of the longitudinal, $Z_{11}(t; \mathbf{a} - \mathbf{b})$, and transverse, $Z_{22}(t; \mathbf{a} - \mathbf{b})$, displacements of two particles in a 2-D conductivity field with $\sigma_f^2 = 0.5$ and $I_{f1} = I_{f2}$ at two dimensionless times after the injection, $t_n = tU/I_{f2} = 5$ and $t_n = 10$, and for three Peclet numbers: $Pe = UI_{f1}/D_d = \infty$, $Pe = 250$ and $Pe = 25$, versus the initial separation: $\mathbf{a} - \mathbf{b} = (0, a_2 - b_2)$ of the particles. Lines and symbols refer to $Z_{ii}(t; \mathbf{a} - \mathbf{b})$ derived from first-order approximations (equation (15)), and from distributions of simulated particle trajectories, respectively.

The approximation of the concentration variance, $\sigma_C^2(x_1, t)$, was calculated in two different ways. In the first procedure we used the distribution of the backward trajectories (equation (22)):

$$\sigma_C^2(x_1, t) = \int_{L_1}\int_{L_1} \frac{1}{\sqrt{(2\pi)^2(X_{11}^2(t) - Z_{11}^2(t; \mathbf{0}))}} \cdot \exp\left(-\frac{1}{2}\left\{[a_1 - (x_1 - Ut)]^2 X_{11}(t) - 2[a_1 - (x_1 - Ut)][b_1 - (x_1 - Ut)]Z_{11}(t; \mathbf{0}) + [b_1 - (x_1 - Ut)]^2 X_{11}(t)\right\}\right) \cdot [X_{11}^2(t) - Z_{11}^2(t; \mathbf{0})]^{-1}\, da_1\, db_1 - \langle C(x_1, t)\rangle^2 \quad (28)$$

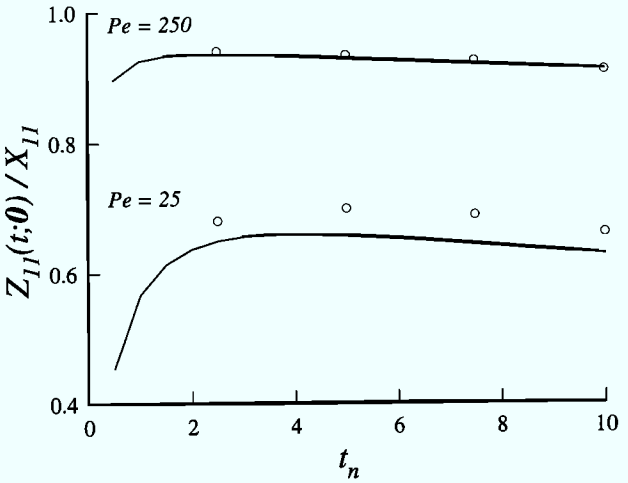

Figure 5. Correlation of the longitudinal trajectories of two microscopic particles, which resided initially in the same macroscopic volume, $Z_{11}(t, \mathbf{0})/X_{11}(t)$, in a 2-D conductivity field with $\sigma_f^2 = 0.5$ and $I_{f1} = I_{f2}$ for $Pe = UI_{f1}/D_d = 250$ versus dimensionless time, $t_n = tU/I_{f1}$. Lines and symbols refer to $Z_{11}(t, \mathbf{0})/X_{11}(t)$ derived from first-order approximations (equations (13) and (15)) and from distributions of simulated particle trajectories, respectively.

In the second procedure, $\langle C(x_1, t)^2 \rangle$ was calculated from (11) assuming that $\Phi_{XY}[\mathbf{x}, \mathbf{x}; t, (a_1, a_2), (b_1, b_2)] \approx \Phi_{XY}[\mathbf{x}, \mathbf{x}; t, (0, a_2), (0, b_2)]$.

The results illustrate that $\langle C(x_1, t) \rangle$ and $\sigma_C(x_1, t)$ can be fairly well predicted from the first-order approximations. However, the $\sigma_C(x_1, t)$ approximations seem to underestimate the simulated $\sigma_C(x_1, t)$, especially for smaller *Pe* and larger travel times. The procedure based on the backward trajectories yields better results. This might be explained by the fact that for a large injection surface this procedure requires neither information on the covariance of the trajectory coordinates of particles that were initially separated at the macroscopic scale nor information on the covariance of the transverse displacements, $Z_{22}(t; \mathbf{a} - \mathbf{b})$. Deviations between approximated $Z_{ii}(t; \mathbf{a} - \mathbf{b})$ and $Z_{ii}(t; \mathbf{a} - \mathbf{b})$ derived from simulated particle trajectories for $\mathbf{a} - \mathbf{b} \neq 0$ might explain the deviations for the second procedure in which these errors are accumulated in the calculation of the integral in (11).

The coefficient of variation of the concentrations along a line transverse to the mean flow direction at the center of mass of the plume, $CV_{Cp} = \sigma_{Cp}/\langle C \rangle$, are shown in Figure 7 for different travel times. Figure 7 illustrates that the first-order trajectory approximations predict, after a certain travel time, a decline of CV_{Cp} with increasing travel times, although very slow (for 2D flow: $CV_C \sim 1/\sqrt{t}$ [*Fiori and Dagan*, 2000]). The predicted decrease of CV_{Cp} by the Lagrangian approach is consistent with predictions of CV_{Cp} based on an Eulerian analysis of convective-dispersive transport in random Darcian velocity fields [e.g., *Andričević*, 1998; *Kapoor and Kitanidis*, 1998], but the Lagrangian and Eulerian approaches lead to different predictions of the rate at which CV_{Cp} decreases. However, CV_{Cp} derived from transport simulations did not decrease with increasing travel time, which is similar to the behavior of the CV_{Cp} in case of zero local scale dispersion. A similar behavior of CV_{Cp} with t was predicted by *Zhang and Neuman* [1996, Figure 3] using a higher-order approximation of an exact Eulerian-Lagrangian theory of advective dispersive transport in random velocity fields.

Whether the concentration variance, $\sigma_C^2(x_1, t)$, is a unimodal or bimodal distribution with x_1, can be evaluated by calculating the second derivative of (28) versus x_1. The distribution $\sigma_C^2(x_1, t)$ is uniform for $Z_{11}(t; \mathbf{0})/X_{11}(t) - CV_{Cp}^2 < 0$ and bimodal for $Z_{11}(t; \mathbf{0})/X_{11}(t) - CV_{Cp}^2 > 0$ [*Fiori and Dagan*, 2000]. From Figures 5 and 7 follows that for the considered travel times in the numerical simulations, $\sigma_C^2(x_1, t)$ is a uniform distribution for $Pe = 2500$ and $Pe = 250$, and a bimodal distribution for $Pe = 25$. This is consistent with the first-order predictions and the distributions of $\sigma_C^2(x_1, t)$ in Figure 6. From (28) follows that for small L_1 and a finite *Pe*:

$$CV_{Cp} \approx \left(\frac{1}{\sqrt{1 - (Z_{11}(t; \mathbf{0})/X_{11}(t))^2}} - 1 \right)^{0.5}. \quad (29)$$

Therefore the first-order approximation of $Z_{11}(t; \mathbf{0})/X_{11}(t) - CV_{Cp}^2$ is positive and the distribution of $\sigma_C^2(x_1, t)$ bimodal for sufficiently large times and a finite *Pe*. This is in qualitative agreement with predictions by the Eulerian approach in which it is conjectured that the $\sigma_C^2(x_1, t)$ distribution reflects at large times the squared gradient of the mean concentration field [*Andričević*, 1998; *Kapoor and Kitanidis*, 1998].

4.3. Concentration Variance and Spatial Covariance in Isotropic and Anisotropic Conductivity Fields

In Figure 8 the spatial covariance of the concentrations along a line perpendicular to the mean flow direction at the center of the plume, $C_{CC}[(x_1 = Ut, x_2), (y_1 = Ut, y_2 = x_2 + lagx_2); t]$ and along a line parallel to the mean flow direction, $C_{CC}[(x_1 = Ut, x_2), (y_1 = Ut + lagx_1, y_2 = x_2); t]$ are shown for the isotropic field when the plume has traveled over a distance $I_{f1} = 2.5$, $I_{f1} = 5$, and $I_{f1} = 10$. The effect of the local scale dispersion on the concentration covariance is shown in Figure 9, whereas Figure 10 illustrates the effect of the variability and spatial correlation of the conductivity field on the concentration spatial covariance. In Figure 10 the spatial concentration covariance in the isotropic and the anisotropic fields 1 and 2 are shown when the plume has traveled over a distance 5 I_{f2} (I_{f2} is the same for the three conductivity fields). At that travel time, the spatial spreading of the plumes in the direction of the mean flow, $X_{11}(t)$, is nearly identical in the three conductivity fields and the Peclet number, $Pe_T = I_{f2} U/D_d = 250$ was constant for the transport simulations in the three conductivity fields.

Note in Figures 8, 9, and 10 that the first-order approximations predict the spatial concentration covariance fairly well. Second, the covariance of the concentration in the direction of the mean flow is mainly determined by the spreading of the plumes in the mean flow direction since the distance over which concentrations are correlated scales with $\sqrt{X_{11}(t)}$ (Figure 8). The spatial covariance in the direction transverse to the mean flow depends on the correlation scale of the conductivity in the transverse to flow direction and on the local scale dispersion. Important in Figure 10 is that for a given spreading of the plume in the direction of the mean flow, $X_{11}(t)$, more or less the same variance and spatial covariance of the local concentrations are obtained for different structures of the hydraulic conductivity field. In addition to the concentration covariances in the hydraulic conductivity fields, in which transport was simulated, we show in Figure 10 also first-order predictions of concentration covariances for two other extreme conductiv-

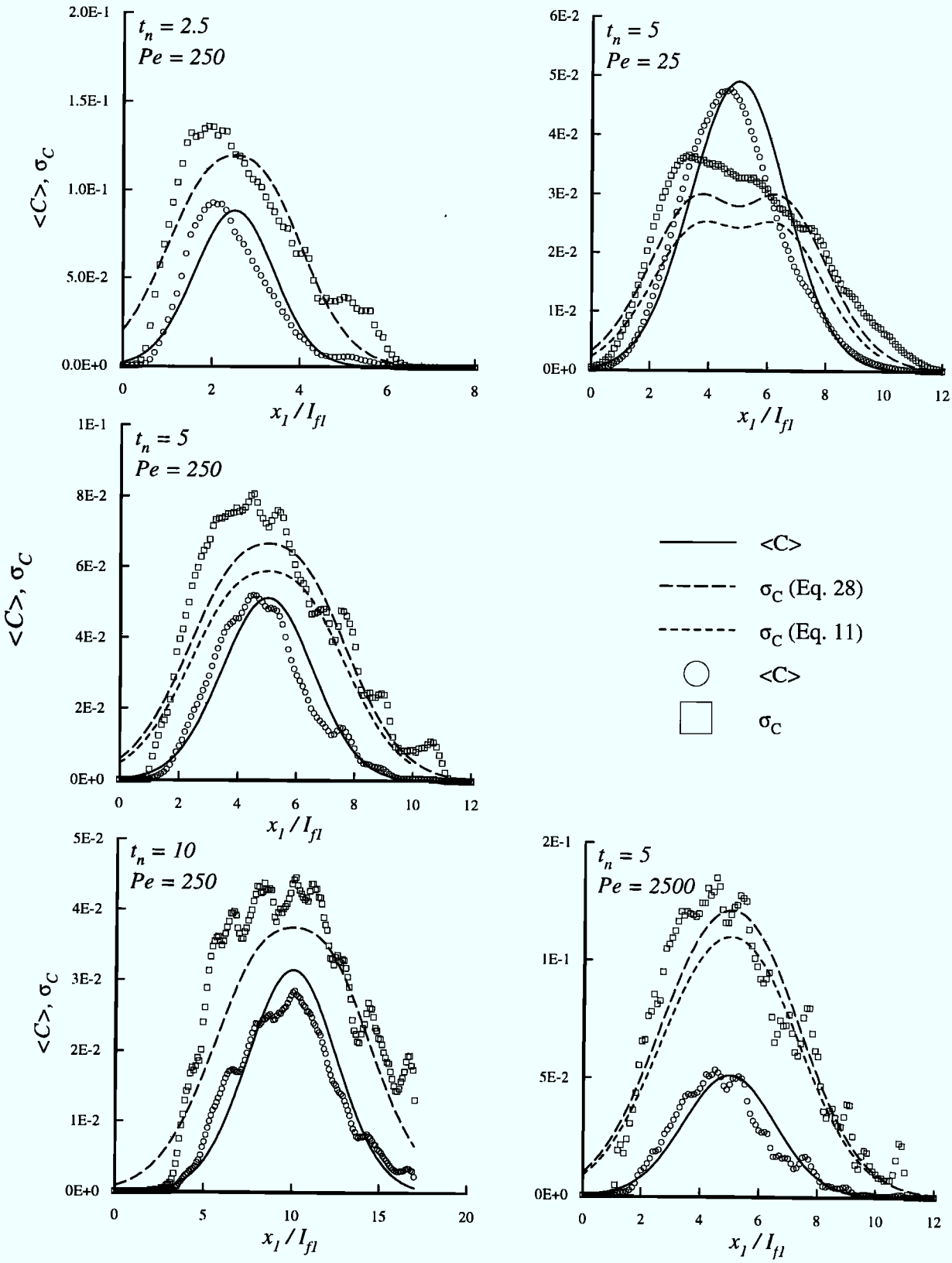

Figure 6. Averages $\langle C(x_1, t)\rangle$ and standard deviations, $\sigma_C(x_1, t)$, of concentrations along lines perpendicular to the mean flow direction in a 2-D conductivity field with $\sigma_f^2 = 0.5$ and $I_{f1} = I_{f2}$, at dimensionless time $t_n = tU/I_{f1} = 2.5$, $t_n = 5$, and $t_n = 10$, and for $Pe = UI_{f1}/D_d = 25$, $Pe = 250$, and $Pe = 25$, versus x_1/I_{f1}. Lines refer to first order approximations of $\langle C(x_1, t)\rangle$ (equation (27)) and of $\sigma_C(x_1, t)$ using either (28) (backward trajectory pdf) or (11) for an infinitely elongated injection volume $\mathbf{V_0}$ ($L_1 \ll I_{f1}$; $L_2 = \infty$), and symbols to $\langle C(x_1, t)\rangle$ and $\sigma_C(x_1, t)$ derived from transport simulations in 10 realizations of the conductivity field for the initial conditions given in the text.

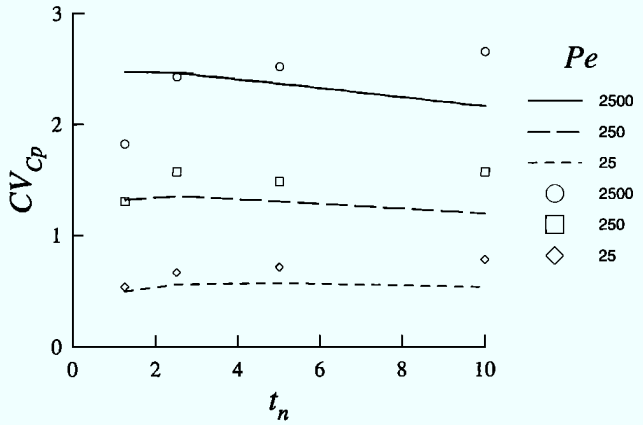

Figure 7. Coefficient of variation of the concentrations along a line perpendicular to the mean flow direction at the center of the plume, $CV_{Cp}(x_1 = Ut, t)$, in a 2-D conductivity field with $\sigma_f^2 = 0.5$ and $I_{f1} = I_{f2}$, for $Pe = UI_{f1}/D_d = 2500$, $Pe = 250$, and $Pe = 25$, versus dimensionless time, $t_n = tU/I_{f1}$. Lines refer to first-order approximations of CV_{Cp} for an infinitely elongated injection volume V_0 ($L_1 \ll I_{f1}$; $L_2 = \infty$) (equations (27) and (28)), and symbols to CV_{Cp} derived from transport simulations in 10 realizations of the conductivity field for the initial conditions given in the text, respectively.

ity structures in which longitudinal spreading of the plume is nearly identical to that in the other fields at the considered travel time: one structure with $I_{f1} = 20\ I_{f2}$ ($e = 0.05$) and $\sigma_f^2 = 0.1165$ and one with $I_{f1} = 0.05\ I_{f2}$ ($e = 20$) and $\sigma_f^2 = 9.36$. The Peclet number ($Pe_T = I_{f2}U/D_{d22} = 250$) in these two extreme conductivity field structures was the same as in the other fields. The relatively large similarity of the concentration structures in these quite different conductivity structures indicates that parameters which characterize the conductivity structures: the anisotropy ratio, $e = I_{f2}/I_{f1}$, of the spatial covariance function and the variance, σ_f^2, of the $\log_e$ transformed hydraulic conductivity, cannot be determined unequivocally from the spatial structure of local concentrations at a single travel time. In these examples the anisotropy ratio e was changed by changing the correlation length of the hydraulic conductivity in the mean flow direction, I_{f1}, whereas I_{f2} and D_d were kept constant and the concentration (co)variance was for a given $X_{11}(t)$ relatively insensitive to changes of I_{f1} and σ_f^2. This illustrates that the reduction of the concentration variance due to local scale dispersion is controlled rather by the Peclet number, $Pe_T = I_{f2}U/D_d$, which was kept constant for the different structures of the conductivity field, than by $Pe = I_{f1}U/D_d$. As a consequence, the local dispersion rate in the direction transverse to flow determines the concentration variance dissipation. In our simulations, we considered an isotropic local scale dispersion tensor with $D_{d11} = D_{d22}$. However, the finding that the local dispersion rate in the transverse to flow direction determines the concentration dissipation indicates that this process is mainly determined by the transverse component of the local scale dispersion tensor, D_{d22}.

The small effect of σ_f^2 and e on the relative variability of local concentrations can be further illustrated by CV_C at the center of the plume, CV_{Cp}, which is predicted by (29). The ratio $Z_{11}(t; \mathbf{0})/X_{11}(t)$ can be written in terms of dimensionless variables:

$$\frac{Z_{11}(t; \mathbf{0})}{X_{11}(t)} = \frac{H(t_n, e, Pe)}{F(t_n, e, Pe) + \dfrac{2t_n}{\sigma_f^2 e\ Pe}} \tag{30}$$

with $t_n = tU/I_{f1}$ and $H(t_n, e, Pe)$ and $F(t_n, e, Pe)$ are given in Appendix A (equations (A3) and (A4)). The second term in the denominator is the contribution of the local scale dispersion to the total spreading of the plume, $X_{11}(t)$. This term can be neglected when $F(t_n, e, Pe) - H(t_n, e, Pe) \gg 2t_n/(\sigma_f^2\ e\ Pe)$, which is fulfilled when the spreading of a locally injected plume is much larger than the spreading of a local plume in a homogeneous velocity field due to local scale dispersion, that is when $\langle \Sigma_{11}(t) \rangle \gg 2D_d t$. When the term can be neglected, $Z_{11}(t; \mathbf{0})/X_{11}(t)$ is not a function of σ_f^2. In Figure 11a, $H(t_n, e, Pe)/F(t_n, e, Pe)$ is plotted versus $t_{nT} = tU/I_{f2}$ for $Pe_T = 25$, 250, and 2500 and a range of e values. A plot versus t_{nT} rather than versus t_n is shown since mixing is mainly determined by the spatial correlation of the conductivity and the velocity in the direction transverse to the flow. Figure 11b shows CV_{Cp}, which is calculated using the approximation $Z_{11}(t; \mathbf{0})/X_{11}(t) \approx H(t_n, e, Pe)/F(t_n, e, Pe)$, and CV_{Cp}, which is calculated for a certain σ_f^2 and e, whereby e and σ_f^2 were chosen so that $X_{11}(t_{nT})$ was identical for all pairs σ_f^2 and e and equal to $X_{11}(t_{nT})$ for the case $\sigma_f^2 = 0.5$ and $e = 1$. For relatively large t_{nT} the approximation $Z_{11}(t; \mathbf{0})/X_{11}(t) \approx H(t_n, e, Pe)/F(t_n, e, Pe)$ can be used to predict CV_{Cp}. Since the ratio $H(t_n, e, Pe)/F(t_n, e, Pe)$ when plotted versus t_{nT} depends only weakly on e (Figure 11a) the approximation of CV_{Cp} is nearly independent of σ_f^2 and e (Figure 11b) and hence of $X_{11}(t)$ for large t_{nT}. It should be noted that this only holds for finite Pe since for an infinite Pe, CV_{Cp} increases with increasing $X_{11}(t)$. For relatively small t_{nT}, $2t_n/(\sigma_f^2\ e\ Pe)$ cannot be neglected. However, for a given $X_{11}(t_{nT})$, CV_{Cp} is relatively independent of the pair (σ_f^2, e), also for smaller t_{nT}.

The analysis of CV_{Cp} and the spatial covariance of concentrations along a line perpendicular to the mean flow direction illustrated that for a given $X_{11}(t)$, these parameters are predominantly determined by Pe_T and I_{f2}. As a consequence, the local scale transverse dispersion, D_{d22}, and I_{f2} may be derived from the local spatial structure of the concentration field. The ratio $I_{f2}/D_{d22} \sim Pe_T$ determines the concentration variance whereas the scale over which the concentrations are correlated is determined by I_{f2} (e.g., Figure 10).

5. Summary and Conclusions

In this paper, we derived in a Lagrangian framework the relations between the spatial covariance of local concentrations and the spatial covariance of the $\log_e$ transformed hydraulic conductivity and the local scale dispersion. In contrast to previous derivations [e.g., *Fiori and Dagan*, 2000] we consider first the concentration field in one realization of the hydraulic conductivity and corresponding Darcian velocity field. This concentration field is obtained from the distribution of the trajectories of microscopic solute particles, $\phi(\mathbf{x})$, in one specific realization of the Darcian velocity field for all realizations of the Wiener process that represents the local scale dispersion process. In line with the perception of the effect of local scale dispersion on the dilution of the injected tracer concentration, this procedure predicts a dilution of the injected concentration due to a synergetic effect of local scale dispersion and variations of advection velocity at a macroscopic scale. This synergetic effect leads, for the same local scale dispersion

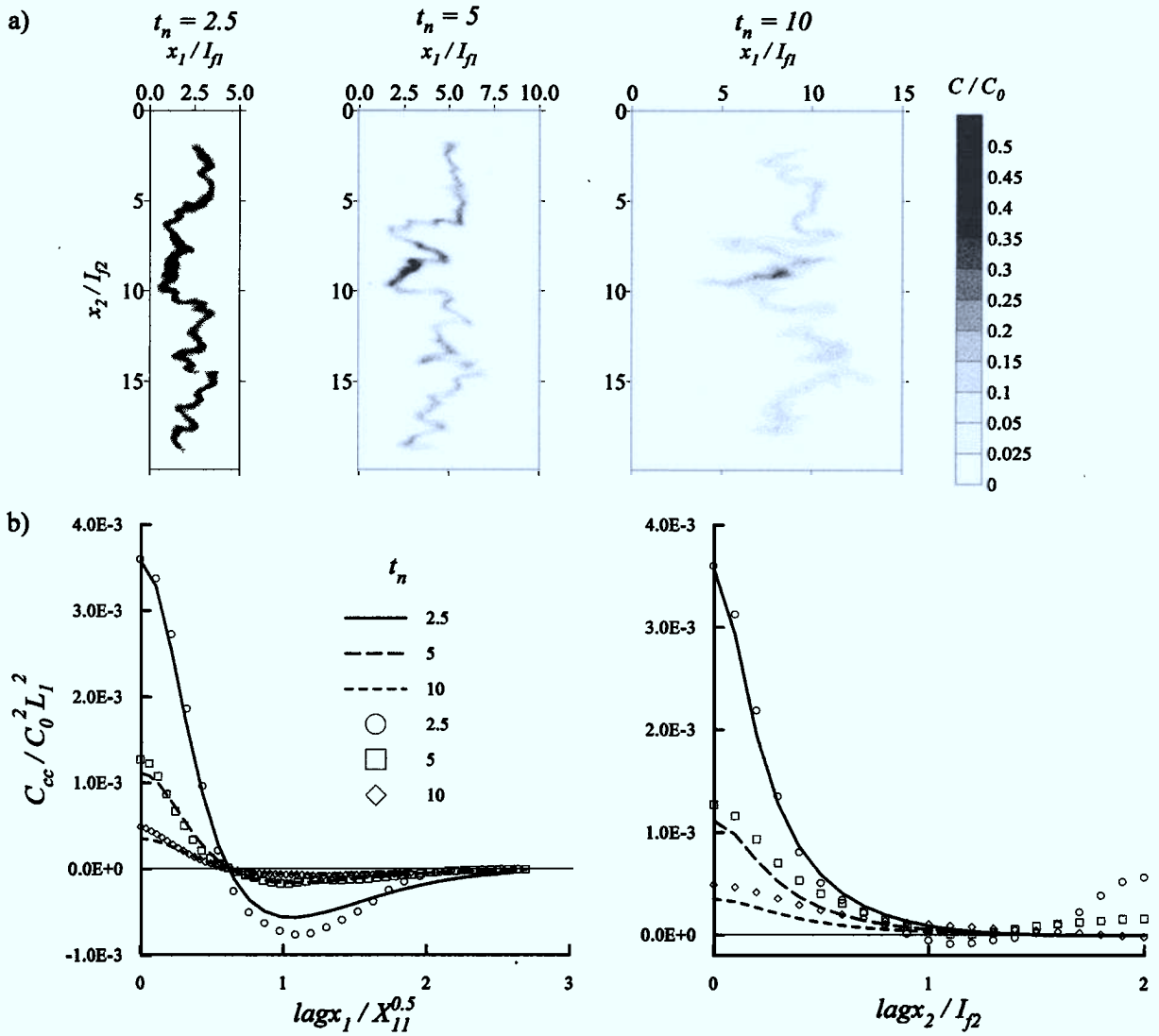

Figure 8. The effect of travel time on the concentration covariance: (a) illustration of simulated concentration patterns, and (b) spatial covariance of concentrations along a line parallel to the mean flow direction (x_1), $C_{CC}[(x_1 = Ut, x_2), (y_1 = Ut + lagx_1, y_2 = x_2)]$ versus $lagx_2/X_{11}(t)^{0.5}$, and along a line transverse to the mean flow direction $(x_2)C_{CC}[(x_1 = Ut, x_2), (y_1 = Ut, y_2 = x_2 + lagx_2)]$ versus $lagx_2/I_{f2}$, in a 2-D conductivity field with $\sigma_f^2 = 0.5$ and $I_{f1} = I_{f2}$, for $Pe = UI_{f1}/D_d = 250$ at three different dimensionless times, $t_n = tU/I_{f1}$. Lines refer to first-order approximations of C_{CC} for an infinitely elongated injection volume $V_0(L_1 \ll I_{f1}; L_2 = \infty)$ (equation (23)), and symbols to C_{CC} derived from transport simulations in 10 realizations of the conductivity field for the initial conditions given in the text.

coefficient, to a larger dilution of the injected tracer concentration in a heterogeneous than in a homogeneous velocity field. In a subsequent step the concentration field is averaged over the different realizations of the conductivity and velocity fields. The ensemble averages $\langle C(\mathbf{x}, t)\rangle$ and $\langle C^2(\mathbf{x}, t)\rangle$ are related to the probability distributions of the particle trajectories, $X(t; \mathbf{a})$, $\Phi_{\mathbf{X}}[\mathbf{X}; t, \mathbf{a}]$, and the joint pdf of the trajectories of two particles, $\mathbf{X}(t; \mathbf{a})$ and $\mathbf{Y}(t; \mathbf{b})$ that are released at, respectively, location $\mathbf{a}$ and $\mathbf{b}$: $\Phi_{\mathbf{XY}}[\mathbf{X}, \mathbf{Y}; t, \mathbf{a}, \mathbf{b}]$. The first two moments of these probability distributions are derived from the variance and spatial covariance of the $\log_e$ transformed conductivity and the local scale dispersion coefficient. Since the evaluation of $\langle C^2(\mathbf{x}, t)\rangle$ involves the integration of $\Phi_{\mathbf{XY}}[\mathbf{X}, \mathbf{Y}; t, \mathbf{a}, \mathbf{b}]$ over $\mathbf{a}$ and $\mathbf{b}$ with $\mathbf{a}$ and $\mathbf{b}$ varying over the entire injection volume $\mathbf{V_0}$ (equation (11)) the calculation of $\langle C^2(\mathbf{x}, t)\rangle$ is quite cumbersome for large injection volumes. However, rather than defining $C(\mathbf{x}, t)$ in terms of the probability that a solute particle, which is injected in $\mathbf{V_0}$ at t_0, reaches the volume $\Delta\mathbf{x}$ centered around $\mathbf{x}$ at time t, one can as well define $C(\mathbf{x}, t)$ in terms of the probability that the backward trajectory of a fictitious solute particle, which is at time t in $\Delta\mathbf{x}$, was at time t_0 in $\mathbf{V_0}$. Linking $\langle C(\mathbf{x}, t)\rangle$ and $\langle C^2(\mathbf{x}, t)\rangle$ to the distribution of backward trajectories dramatically simplifies the calculations of $\langle C^2(\mathbf{x}, t)\rangle$ for large injection volumes (equation (22)). A comparison between variances and covariances of numerically simulated concentrations in generated random conductivity fields and predictions based on a first-order approximation of the particle trajectories illustrated that predictions based on

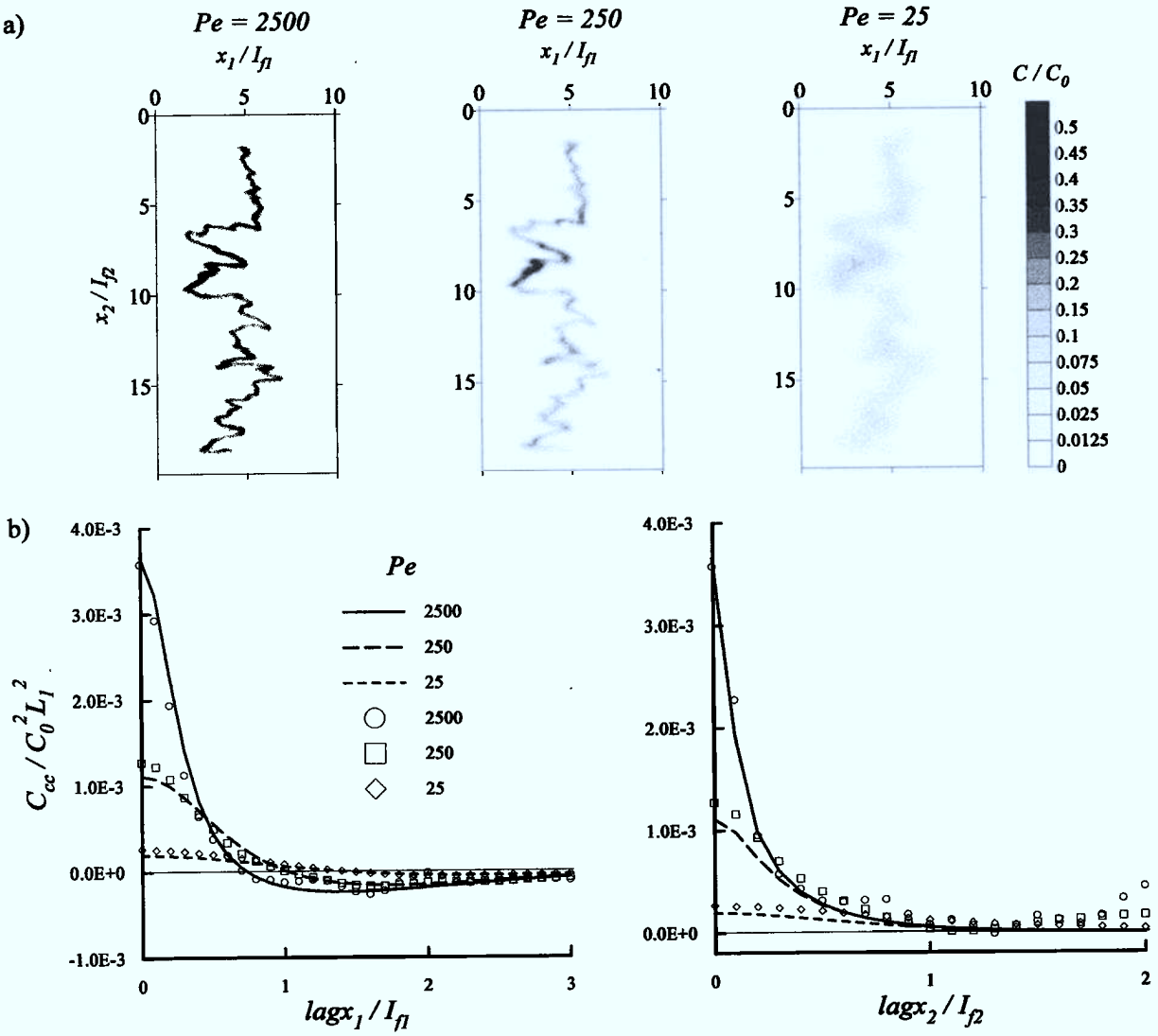

Figure 9. The effect of local scale dispersion on the concentration covariance: (a) illustration of simulated concentration patterns, and (b) spatial covariance of concentrations along a line parallel to the mean flow direction (x_1), $C_{CC}[(x_1 = Ut, x_2), (y_1 = Ut + lagx_1, y_2 = x_2)]$ versus $lagx_1/I_{f2}$ and along a line transverse to the mean flow direction (x_2), $C_{CC}[(x_1 = Ut, x_2), (y_1 = Ut, y_2 = x_2 + lagx_2)]$ versus $lagx_2/I_{f2}$, in a 2-D conductivity field with $\sigma_f^2 = 0.5$ and $I_{f1} = I_{f2}$, at $t_n = tU/I_{f1} = 5$, for $Pe = UI_{f1}/D_d = 2500$, $Pe = 250$, and $Pe = 25$. Lines refer to first-order approximations of C_{CC} for an infinitely elongated injection volume $V_0(L_1 \ll I_{f1}; L_2 = \infty)$ (equation (23)), and symbols to C_{CC} derived from transport simulations in 10 realizations of the conductivity field for the initial conditions given in the text.

the distribution of backward solute trajectories are also more accurate than predictions that are based on the integration of $\Phi_{XY}[\mathbf{X}, \mathbf{Y}; t, \mathbf{a}, \mathbf{b}]$ over $\mathbf{V_0}$. The procedure based on the backward trajectories is not prone to errors that are caused by the approximation of the two-particle trajectory covariances, $Z_{ii}(t; \mathbf{a} - \mathbf{b})$ for large separation distances of the initial particle locations. For relatively large $\mathbf{a} - \mathbf{b}$ the first-order approximations underestimated the simulated two-particle trajectory covariances $Z_{ii}(t; \mathbf{a} - \mathbf{b})$, and these errors are accumulated in the integration of $\Phi_{XY}(\mathbf{X}, \mathbf{Y}; t, \mathbf{a}, \mathbf{b})$ over $\mathbf{V_0}$.

The predictions of the concentration covariance based on the distribution of first-order approximate backward solute trajectories reproduced fairly well the simulated concentration covariance for different structures of the hydraulic conductivity field and different local scale dispersion coefficients. For a given spreading of the plume in the mean flow direction, $X_{11}(t)$, the concentration covariance was relatively independent of anisotropy of the spatial covariance, $e = I_{f2}/I_{f1}$ and the variance, σ_f^2, of the $\log_e$ transformed conductivity. Therefore these parameters cannot be unequivocally determined from the structure of a single solute plume. However, for a given $X_{11}(t)$ the concentration variance and spatial covariance along a line transverse to the mean flow direction can be used to determine the correlation length of the hydraulic conductivity in the transverse to flow direction, I_{f2}, and the local scale transverse dispersion, D_{d22}. In the case of 3-D flow in a horizontally isotropic medium this implies that the correlation scale in the horizontal direction, $I_{f1} = I_{f2}$, could be inferred from the correlation of the local concentrations in the horizontal direction transverse to the mean flow direction. There-

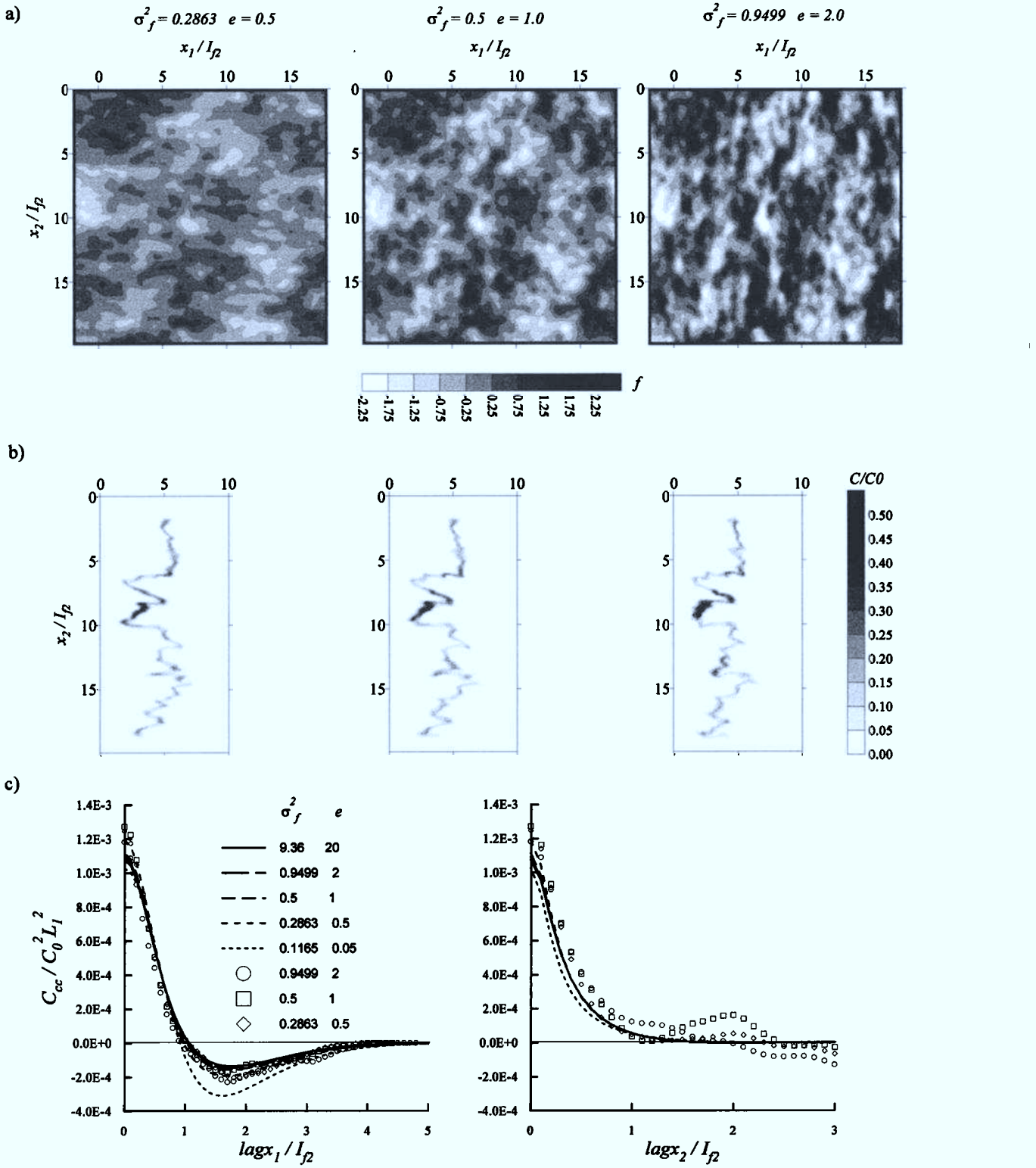

Figure 10. The effect of the variance, σ_f^2, and anisotropy of the spatial covariance, $e = I_{f2}/I_{f1}$, of the $\log_e$ transformed hydraulic conductivity on the concentration covariance: (a) illustration of the generated fields of fluctuations of the $\log_e$ transformed conductivity, f, for three different pairs (σ_f^2, e) with constant I_{f2}, (b) illustration of simulated concentration patterns in these conductivity fields, and (c) spatial covariance of concentrations along a line parallel to the mean flow direction (x_1), $C_{CC}[(x_1 = Ut, x_2), (y_1 = Ut + lagx_1, y_2 = x_2)]$ versus $lagx_1/I_{f2}$ and along a line transverse to the mean flow direction (x_2), $C_{CC}[(x_1 = Ut, x_2), (y_1 = Ut, y_2 = x_2 + lagx_2)]$ versus $lagx_2/I_{f2}$, in these conductivity fields at $t_{nT} = tU/I_{f2} = 5$ for $Pe_T = UI_{f2}/D_d = 250$. Lines refer to first-order approximations of C_{CC} for an infinitely elongated injection volume $V_0(L_1 \ll I_{f1}; L_2 = \infty)$ (equation (23)), and symbols to C_{CC} derived from transport simulations in 10 realizations of the conductivity fields for the initial conditions given in the text.

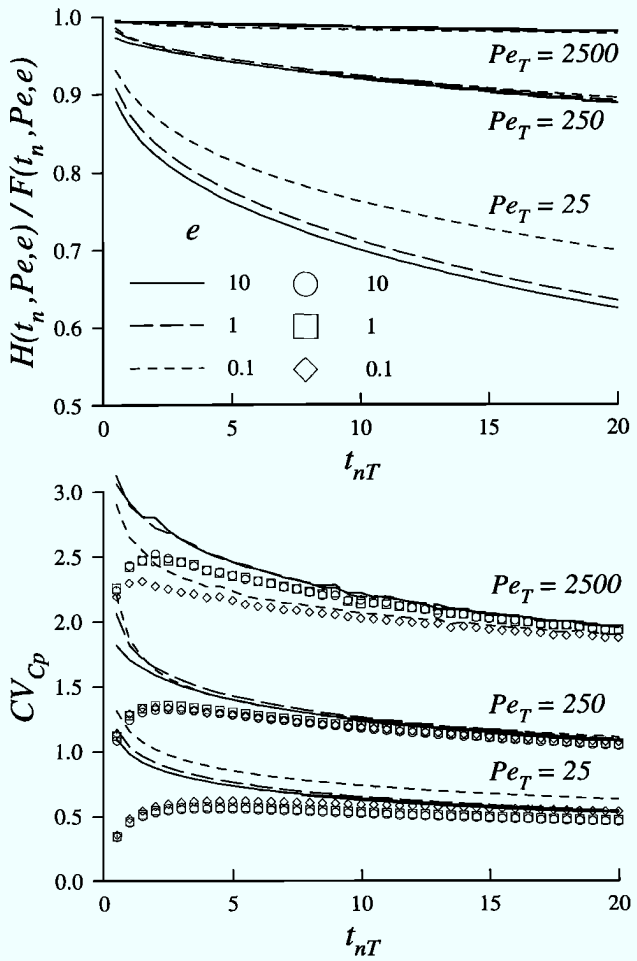

Figure 11. The effect of the variance, σ_f^2, and anisotropy of the spatial covariance, $e = I_{f2}/I_{f1}$, of the $\log_e$ transformed hydraulic conductivity on the coefficient of variation of concentrations at the center of the plume, CV_{Cp}: (a) $H(t_n, Pe, e)/F(t_n, Pe, e)$ (equations (A3) and (A4)) and (b) CV_{Cp} versus $t_{nT} = tU/I_{f2}$ for $e = 0.1$, $e = 1$, and $e = 10$ and for $Pe_T = UI_{f2}/D_d = 2500$, $Pe_T = 250$, and $Pe_T = 25$. Lines refer to CV_{Cp} calculated with the approximation $Z_{11}(t; \mathbf{0})/X_{11}(t) \approx H(t_n, e, Pe)/F(t_n, e, Pe)$ and symbols to CV_{Cp} calculated from (29) and (30) with σ_f^2 chosen so that for a given t_{nT}, Pe_T and e, $X_{11}(t_{nT}; \sigma_f^2, e, Pe_T) = X_{11}(t_{nT}; \sigma_f^2 = 0.5, e = 1, Pe_T)$.

fore, given I_{f1} and $X_{11}(t)$, σ_f^2 could be derived on the basis of concentration measurements. Since the transverse local scale dispersion is difficult to determine from laboratory scale leaching experiments, the first-order approximate relations to predict the concentration covariance might be helpful to estimate this parameter from the spatial (co)variance of solute concentration in heterogeneous formations. In this paper the spatial distribution of local concentrations was analyzed using a first-order approximate Lagrangian description of transport. Alternatively, this transport description can be used as well to investigate the temporal evolution of local concentrations and to derive the transverse dispersion coefficient from time series of local concentrations (J. Vanderborght and H. Vereecken, Estimation of local scale dispersion from local breakthrough curves during a tracer test in a heterogeneous aquifer: The Lagrangian approach, submitted to *Journal of Contaminant Hydrology*, 2001).

Appendix A

For a mean head gradient, **J**, coinciding with a principal direction of the spatial covariance function of a second-order stationary conductivity field and a locally isotropic dispersion tensor: $D_{d11} = D_{d22}$ and $D_{d12} = D_{d21} = 0$, the variance of the particle trajectory coordinates, $X_{ij}(t)$ and the covariance of the trajectory coordinates of two particles that started at time t_0 at locations **a** and **b**, $Z_{ij}(t; \mathbf{a}, \mathbf{b})$ can be written for 2-D flow as

$$X_{ij}(t_n) = \frac{\sigma_f^2 e J^2 K_G^2 I_{f1}^2}{\theta^2} F_{ij}(t_n, Pe, e) + 2\frac{t_n J^2 K_G^2 I_{f1}^2}{Pe\ \theta^2} \tag{A1}$$

$$Z_{ij}(t_n, \mathbf{a_n} - \mathbf{b_n}) = \frac{\sigma_f^2 e J^2 K_G^2 I_{f1}^2}{\theta^2} H_{ij}(t_n, Pe, e, \mathbf{a_n} - \mathbf{b_n}) \tag{A2}$$

with σ_f^2 the variance of the $\log_e$ transformed conductivity, K_G the geometric mean of conductivity, θ the porosity, J the mean head gradient, I_{f1} the correlation scale of the $\log_e$ transformed conductivity in the direction of the mean gradient, $e = I_{f2}/I_{f1}$ the anisotropy ratio, $t_n = tK_GJ/(\theta I_{f1})$ the dimensionless travel time, $Pe = K_GJI_{f1}/(\theta D_{d11})$ the Peclet number, and $\mathbf{a_n} - \mathbf{b_n} = (\mathbf{a} - \mathbf{b})/I_{f1}$, the normalized distance between the original particle locations. For an exponential covariance of the $\log_e$ transformed conductivities (equation (24)), $F_{ij}(t_n, Pe, e)$ and $H_{ij}(t_n, Pe, e, \mathbf{a_n} - \mathbf{b_n})$ are

$$F_{ij}(t_n, Pe, e) = \frac{2}{\pi}\int_0^\infty \int_0^\pi S_{uiuj}(k, \psi)\Big\{\{-(k/Pe)^2 + \cos^2\psi + \exp(-k^2 t_n/Pe)[((k/Pe)^2 - \cos^2\psi)\cos(kt_n\cos\psi) - 2(k/Pe)\cos\psi\sin(kt_n\cos\psi)]\}[k((k/Pe)^2 + \cos^2\psi)^2]^{-1} + \frac{t_n k/Pe}{(k/Pe)^2 + \cos^2\psi}\Big\}\, d\psi\, dk \tag{A3}$$

$$H_{ij}(t_n, Pe, e, \mathbf{a_n} - \mathbf{b_n}) = \frac{1}{2\pi}\int_0^\infty \int_0^{2\pi} S_{uiuj}(k, \psi) \cdot [1 - 2\cos(kt_n\cos\psi)\exp(-k^2 t_n/Pe) + \exp(-2k^2 t_n/Pe)]\cos[k((a_{1n} - b_{1n})\cos\psi + (a_{2n} - b_{2n})\sin\psi)][k((k/Pe)^2 + \cos^2\psi]^{-1}\, d\psi\, dk \tag{A4}$$

with

$$S_{uiuj}(k, \psi) = \sum_{p=1}^{2}\sum_{q=1}^{2}\delta_{ip}\delta_{iq}\left(\delta_{ip} - \frac{k_i k_q}{k^2}\right) \cdot \left(\delta_{jp} - \frac{k_j k_q}{k^2}\right)\frac{1}{(1 + k^2(\cos^2\psi + e^2\sin^2\psi))^{15}} \tag{A5}$$

and $k_1 = k\cos\psi$ and $k_2 = k\sin\psi$.

Notation

$\mathbf{a}$ Coordinate vector of a point in the injection volume, $\mathbf{V_0}$.

$\mathbf{A}(t'; t, \mathbf{x})$ Coordinate vector at time t' of the location of a fictitious particle that reaches a volume $\Delta\mathbf{x}$ around $\mathbf{x}$ at time t (backward trajectory).

$\mathbf{b}$ Coordinate vector of a point in the injection volume, $\mathbf{V_0}$.

$\mathbf{B}(t'; t, \mathbf{y})$ Coordinate vector at time t' of the location of a fictitious particle that reaches a volume $\Delta\mathbf{y}$ around $\mathbf{y}$ at time t (backward trajectory).

C_0 Initial concentration in the injection volume, $\mathbf{V_0}$, at time t_0.

$C(\mathbf{x}, t)$ Concentration at point x and at time t.

C_p Concentration at the center of the plume.

$C_{zz}(\mathbf{x}, \mathbf{y})$ Spatial covariance between variable z at point $\mathbf{x}$ and at point $\mathbf{y}$.

CV_z Coefficient of variation of variable z.

$\mathbf{D_d}$ Local scale dispersion tensor.

D_{dij} ijth element of the local scale dispersion tensor.

dm Mass of an indivisible microscopic solute particle.

e Anisotropy ratio of the spatial covariance of the $\log_e$ transformed hydraulic conductivity (I_{f2}/I_{f1}).

f Fluctuation of the $\log_e$ transformed conductivity ($f = \log_e(K) - K_G$).

$\mathbf{J}$ Mean gradient vector.

$\mathbf{k}$ Frequency vector.

K Hydraulic conductivity.

K_G Geometric mean of the hydraulic conductivity.

L_i Length of the injection volume in direction i.

$m^2_{(i)}$ Ordered Mahalanobis distance.

$n_0(\mathbf{a})$ Number of particles that are at time $t = t_0$ in $\Delta\mathbf{a}$ centered around $\mathbf{a}$.

$n_0^f(\mathbf{x})$ Number of fictitious particles that are at time t in $\Delta\mathbf{x}$ centered around $\mathbf{x}$ of which backward trajectories are calculated.

$n(\mathbf{x}, t)$ Number of particles that are at time t in $\Delta\mathbf{x}$ centered around $\mathbf{x}$.

$n(\mathbf{x}, t; t_0, \mathbf{a})$ Number of particles that were at time t_0 in $\Delta\mathbf{a}$ centered around $\mathbf{a}$ and at time t in $\Delta\mathbf{x}$ centered around $\mathbf{x}$.

$n^f(\mathbf{a}, t'; t, \mathbf{x})$ Number of fictitious particles that reach at time t in $\Delta\mathbf{x}$ centered around $\mathbf{x}$ and of which the backward trajectory at time t' is in $\Delta\mathbf{a}$ centered around $\mathbf{a}$.

$P(z)$ Probability of z.

Pe Peclet number, defined in terms of the correlation scale of the $\log_e$ transformed conductivity in the direction of the mean flow and the longitudinal local dispersion ($Pe = I_{f1}U/D_{d11}$).

Pe_T Peclet number, defined in terms of the correlation scale of the $\log_e$ transformed conductivity transverse to the mean flow direction and the transverse local dispersion ($Pe = I_{f1}U/D_{d11}$).

$\mathbf{R}(t; t_0, \mathbf{a})$ Coordinate vector of the mean position at time t of particles that were released at time t_0 in one realization of the velocity field in $\Delta\mathbf{a}$ centered around $\mathbf{a}$.

$\mathbf{R_A}(t'; t, \mathbf{x})$ Coordinate vector of the mean position at time t' of fictitious particles in one realization of the velocity field that reach $\Delta\mathbf{x}$ centered around $\mathbf{x}$ at time t.

$\mathbf{S}(t; t_0, \mathbf{b})$ Coordinate vector of the mean position at time t of particles that were released at time t_0 in one realization of the velocity field in $\Delta\mathbf{b}$ centered around $\mathbf{b}$.

$S_{zz}(\mathbf{k})$ Power spectrum of variable z.

t Time.

t_n Normalized time ($t_n = tU/I_{f1}$).

t_{nT} Normalized time ($t_{nT} = tU/I_{f2}$).

t_0 Injection time.

$\mathbf{u}(\mathbf{x})$ Pore water velocity vector at point $\mathbf{x}$.

$\mathbf{U}$ Mean pore water velocity vector.

$\mathbf{V_0}$ Injection volume.

$\mathbf{x}$ Coordinate vector of a point in the flow domain.

$\mathbf{X}(t; t_0, \mathbf{a})$ Coordinate vector at time t of the location of a particle that is injected at time t_0 in a volume $\Delta\mathbf{a}$ around $\mathbf{a}$.

$X_{ij}(t)$ Covariance at time t of the ith and jth coordinate of a particle trajectory in several realizations of the velocity field.

$\mathbf{y}$ Coordinate vector of a point in the flow domain.

$\mathbf{Y}(t; t_0, \mathbf{b})$ Coordinate vector at time t of the location of a particle that is injected at time t_0 in a volume $\Delta\mathbf{b}$ around $\mathbf{b}$.

$Z_{ij}(t; \mathbf{a}, \mathbf{b})$ Covariance at time t of the ith coordinate of a particle that is injected in $\Delta\mathbf{a}$ around $\mathbf{a}$ and the jth coordinate of a particle that is injected in $\Delta\mathbf{b}$ around $\mathbf{b}$ in several realizations of the velocity field.

$\delta(t)$ Dirac function.

δ_{ij} Kronecker delta.

$\Delta\mathbf{a}$ Infinitesimal volume that is centered around $\mathbf{a}$.

Δt Time step used in the particle tracking procedure.

$\Delta\mathbf{x}$ Infinitesimal volume that is centered around $\mathbf{x}$; grid size used in the numerical flow and transport simulations.

$\Delta\mathbf{x_d}$ Diffusive displacement of a particle during a time Δt.

$\phi[\mathbf{X}; \mathbf{R}(t; \mathbf{a}), \Sigma(t; \mathbf{a})]$ Probability density function of $\mathbf{X}(t; t_0, \mathbf{a})$ at time t in one realization of the Darcian velocity field.

$\phi_A[\mathbf{A}; \mathbf{R_A}(t'; t, \mathbf{x}), \Sigma_A(t'; t, \mathbf{x})]$ Probability density function of $\mathbf{A}(t'; t, \mathbf{x})$ at time t' in one realization of the Darcian velocity field.

$\Phi_\mathbf{A}[\mathbf{A}; t, \mathbf{x}]$ Probability density function of $\mathbf{A}(t_0; t, \mathbf{x})$ at time t_0 in all realizations of the Darcian velocity field.

$\Phi_{\mathbf{AB}}[\mathbf{A}, \mathbf{B}; t, \mathbf{x}, \mathbf{y}]$ Joint probability density function of $\mathbf{A}(t_0; t, \mathbf{x})$ and $\mathbf{B}(t_0; t, \mathbf{x})$ at time t_0 in all realizations of the Darcian velocity field.

$\Phi_{\mathbf{R}}[\mathbf{R};\ t,\ \mathbf{a}]$ Probability density function of $\mathbf{R}(t;\ \mathbf{a})$ at time t in all realizations of the Darcian velocity field.

$\Phi_{\mathbf{RS}}[\mathbf{R},\ \mathbf{S};\ t,\ \mathbf{a},\ \mathbf{b}]$ Joint probability density function of $\mathbf{R}(t;\ \mathbf{a})$ and $\mathbf{S}(t;\ \mathbf{b})$ at time t in all realizations of the Darcian velocity field.

$\Phi_{\mathbf{X}}[\mathbf{X};\ t,\ \mathbf{a}]$ Probability density function of $\mathbf{X}(t;\ \mathbf{a})$ at time t in all realizations of the Darcian velocity field.

$\Phi_{\mathbf{XY}}[\mathbf{X},\ \mathbf{Y};\ t,\ \mathbf{a},\ \mathbf{b}]$ Joint probability density function of $\mathbf{X}(t;\ \mathbf{a})$ and $\mathbf{Y}(t;\ \mathbf{b})$ at time t in all realizations of the Darcian velocity field.

σ_z^2 Variance of variable z.

$\Sigma(t;\ \mathbf{a})$ Variance-covariance matrix of the coordinates of $\mathbf{X}(t;\ \mathbf{a})$ in one realization of the Darcian velocity field.

$\Sigma_A(t';\ t,\ \mathbf{x})$ Variance-covariance matrix of the coordinates of $\mathbf{A}(t';\ t,\ \mathbf{x})$ in one realization of the Darcian velocity field.

$\Sigma_R(t)$ Variance-covariance matrix of the coordinates of $\mathbf{R}(t;\ \mathbf{a})$ in all realizations of the Darcian velocity field.

$\Sigma_{\Delta xd}$ Variance-covariance matrix of the coordinates of $\Delta\mathbf{x}_\mathbf{d}$ in all realizations of the Wiener process that represents local scale dispersion.

$\Xi(t)$ Variance-covariance matrix of the coordinates of $\mathbf{X}(t;\ \mathbf{a})$ in all realizations of the Darcian velocity field.

$\langle z \rangle$ Expected value of variable z in all realizations of the Darcian velocity field or ensemble average.

$\hat{z}$ Difference between variable z and its ensemble average.

$\tilde{\mathbf{X}}$ Difference between $\mathbf{X}$ and the expected value of $\mathbf{X}$ in one realization of the Darcian velocity field.

Acknowledgments. I wish to acknowledge the Belgian Fund for Scientific Research. Jan Vanderborght is a Post-Doc research assistant of the Belgian Fund for Scientific Research. I am also grateful to Hannes Flühler and Nadia Ursino for their helpful comments.

References

Andričević, R., Effects of local dispersion and sampling volume on the evolution of concentration fluctuations in aquifers, *Water Resour. Res.*, *34*, 1115–1129, 1998.

Bellin, A., P. Salandin, and A. Rinaldo, Simulation of dispersion in hetergeneous porous formations: Statistics, first-order theories, convergence of computations, *Water Resour. Res.*, *28*, 2211–2227, 1992.

Bellin, A., M. Pannone, A. Fiori, and A. Rinaldo, On transport in porous formations characterized by heterogeneity of evolving scales, *Water Resour. Res.*, *32*, 3485–3496, 1996.

Burr, D. T., E. A. Sudicky, and R. L. Naff, Nonreactive and reactive solute transport in three-dimensional porous media: Mean displacement, plume spreading, and uncertainty, *Water Resour. Res.*, *30*, 791–817, 1994.

Chin, D. A., and T. Wang, An investigation of the validity of first-order stochastic dispersion theories in isotropic porous media, *Water Resour. Res.*, *28*, 1531–1542, 1992.

Cvetkovic, V., and G. Dagan, Transport of kinetically sorbing solute by steady random velocity in heterogeneous porous formations, *J. Fluid Mech.*, *265*, 189–215, 1994.

Dagan, G., Stochastic modeling of groundwater flow by unconditional and conditional probabilities, 2, The solute transport, *Water Resour. Res.*, *18*, 835–848, 1982.

Dagan, G., *Flow and Transport in Porous Formations*, Springer Verlag, New York, 1989.

Dagan, G., The significance of heterogeneity of evolving scales to transport in porous formations, *Water Resour. Res.*, *30*, 3327–3336, 1994.

Dagan, G., and A. Fiori, The influence of pore-scale dispersion on concentration statistical moments in transport through heterogeneous aquifers, *Water Resour. Res.*, *33*, 1595–1605, 1997.

Dagan, G., I. Butera, and E. Grella, Impact of concentration measurements upon estimation of flow and transport parameters: The Lagrangian approach, *Water Resour. Res.*, *32*, 297–306, 1996.

Fiori, A., Finite-Peclet extensions of Dagan's solution to transport in anisotropic heterogeneous formations, *Water Resour. Res.*, *32*, 193–198, 1996.

Fiori, A., and G. Dagan, Concentration fluctuations in transport by groundwater: Comparison between theory and field experiments, *Water Resour. Res.*, *35*, 105–112, 1999.

Fiori, A., and G. Dagan, Concentration fluctuations in aquifer transport. A rigorous first-order solution and applications, *J. Contam. Hydrol.*, *45*, 139–163, 2000.

Gelhar, L. W., *Stochastic Subsurface Hydrology*, Prentice Hall, Englewood Cliffs, N. J., 1993.

Graham, W., and D. McLaughlin, Stochastic analysis of nonstationary subsurface solute transport, 1, Unconditional moments, *Water Resour. Res.*, *25*, 215–232, 1989.

Gutjahr, A. L., S. Hatch, and B. Bullard, *Random Field Generation, Conditional Simulation, and Flow Modeling Using the Fast Fourier Transform*, N. M. Inst. of Min. and Technol., Socorro, 1995.

Indelman, P., and Y. Rubin, Solute transport in nonstationary velocity fields, *Water Resour. Res.*, *32*, 1259–1267, 1996.

Jobson, J. D., *Applied multivariate data analysis*, vol. II, *Categorical and Multivariate Methods*, Springer-Verlag, New York, 1992.

Kapoor, V., and L. W. Gelhar, Transport in three dimensionally heterogeneous aquifers, 1, Dynamics of concentration fluctuations, *Water Resour. Res.*, *30*, 1775–1788, 1994a.

Kapoor, V., and L. W. Gelhar, Transport in three dimensionally heterogeneous aquifers, 2, Predictions and observations of concentration fluctuations, *Water Resour. Res.*, *30*, 1789–1801, 1994b.

Kapoor, V., and P. K. Kitanidis, Concentration fluctuations and dilution in two-dimensionally periodic heterogeneous porous media, *Transp. Porous Media*, *22*, 91–119, 1996.

Kapoor, V., and P. K. Kitanidis, Concentration fluctuations and dilution in aquifers, *Water Resour. Res.*, *34*, 1181–1193, 1998.

Naff, R. L., D. F. Haley, and E. A. Sudicky, High-resolution Monte Carlo simulation of flow and conservative transport in heterogeneous porous media, 1, Methodology and flow results, *Water Resour. Res.*, *34*, 663–677, 1998a.

Naff, R. L., D. F. Haley, and E. A. Sudicky, High-resolution Monte Carlo simulation of flow and conservative transport in heterogeneous porous media, 2, Transport results, *Water Resour. Res.*, *34*, 679–697, 1998b.

Neuman, S. P., Eulerian-Lagrangian theory of transport in space-time nonstationary velocity fields: Exact nonlocal formalism by conditional moments and weak approximations, *Water Resour. Res.*, *29*, 633–645, 1993.

Neuman, S. P., On advective transport in fractal permeability and velocity fields, *Water Resour. Res.*, *31*, 1455–1460, 1995.

Pannone, M., and P. K. Kitanidis, Large-time behavior of concentration variance and dilution in heterogeneous formations, *Water Resour. Res.*, *35*, 623–634, 1999.

Roth, K., and K. Hammel, Transport of conservative chemical through an unsaturated two-dimensional Miller-similar medium with steady state flow, *Water Resour. Res.*, *32*, 1653–1663, 1996.

Rubin, Y., The spatial and temporal moments of tracer concentration in disordered porous media, *Water Resour. Res.*, *27*, 2845–2854, 1991.

Rubin, Y., and S. Ezzedine, The travel times of solutes at the Cape Cod Tracer Experiment: Data analysis, modeling, and structural parameters inference, *Water Resour. Res.*, *33*, 1537–1547, 1997.

Salandin, P., and V. Fiorotto, Solute transport in highly heterogeneous aquifers, *Water Resour. Res.*, *34*, 949–961, 1998.

Šimůnek, J., T. Vogel, and M. T. van Genuchten, The SWMS_2D code for simulating water flow and solute transport in two-dimensional variably saturated media, *Res. Rep. 132*, U.S. Salinity Lab., Agri. Res. Serv., U.S. Dep. of Agric., Riverside, Calif., 1994.

Vanderborght, J., and H. Vereecken, Analyses of locally measured

bromide breakthrough curves from a natural gradient tracer experiment at Krauthausen, *J. Contam. Hydrol.*, *48*, 23–43, 2001.

Vomvoris, E. G., and L. W. Gelhar, Stochastic analysis of the concentration variability in a three dimensionally heterogeneous aquifer, *Water Resour. Res.*, *26*, 2591–2602, 1990.

Zhang, D., and S. P. Neuman, Effect of local dispersion on solute transport in randomly heterogeneous media, *Water Resour. Res.*, *32*, 2715–2723, 1996.

J. Vanderborght, Institute of Chemistry and Dynamics of the Geosphere ICG-4, Forschungszentrum Jülich, D-52425 Jülich, Germany.

(Received June 15, 2000; revised December 29, 2000;
accepted December 29, 2000.)